

To appear in *The Astronomical Journal*, June 2004

# An IRAS High Resolution Image Restoration (HIRES) Atlas of All Interacting Galaxies in the IRAS Revised Bright Galaxy Sample

Jason A. Surace

*SIRTF Science Center, MS 220-6, California Institute of Technology, Jet Propulsion Laboratory,  
Pasadena, CA 91125*

jason@ipac.caltech.edu

D. B. Sanders

*University of Hawaii, Institute for Astronomy, 2680 Woodlawn Dr., Honolulu, HI, 96822*

sanders@ifh.hawaii.edu

and

Joseph M. Mazzarella

*Infrared Processing and Analysis Center, MS 100-22, California Institute of Technology, Jet Propulsion  
Laboratory, Pasadena, CA 91125*

mazz@ipac.caltech.edu

## ABSTRACT

The importance of far-infrared observations in our understanding of extreme activity in interacting and merging galaxies has been illustrated by many studies. Even though two decades have passed since its launch, the most complete all-sky survey to date from which far-infrared selected galaxy samples can be chosen is still that of the Infrared Astronomical Satellite (IRAS). However, the spatial resolution of the IRAS all-sky survey is insufficient to resolve the emission from individual galaxies in most interacting galaxy pairs, and hence previous studies of their far-IR properties have had to concentrate either on global system properties or on the properties of very widely separated and weakly interacting pairs. Using the HIRES image reconstruction technique, it is possible to achieve a spatial resolution ranging from  $30''$  to  $1.5'$  (depending on wavelength and detector coverage), which is a fourfold improvement over the normal resolution of IRAS. This is sufficient to resolve the far-infrared emission from the individual galaxies in many interacting systems detected by IRAS, which is very important for meaningful comparisons with single, isolated galaxies.

We present high-resolution 12, 25, 60, and  $100\ \mu\text{m}$  images of 106 interacting galaxy systems contained in the IRAS Revised Bright Galaxy Sample (RBGS, Sanders et al. 2003), a complete sample of all galaxies having a  $60\ \mu\text{m}$  flux density greater than 5.24 Jy. These systems were selected to have at least two distinguishable galaxies separated by less than three average galactic diameters, and thus we have excluded very widely separated systems and very advanced mergers. Additionally, some systems have been included which are more than three galactic diameters apart, yet have separations less than  $4'$ , and which are thus likely to suffer from confusion in the RBGS.

The new complete survey has the same properties as the prototype survey of Surace et al. (1993). We find no increased tendency for infrared-bright galaxies to be associated with other infrared bright galaxies among the widely separated pairs studied here. We find small enhancements in far-infrared activity in multiple galaxy systems relative to RBGS non-interacting galaxies with the same blue luminosity distribution. We also find no differences in infrared activity (as measured by infrared color and luminosity) between late and early-type spiral galaxies.

*Subject headings:* atlases — techniques: image processing — galaxies: interactions — infrared: galaxies — infrared: general

## 1. Introduction

In the last two decades it has become apparent that interactions between galaxies can play a significant role in their evolution. From the early dynamical simulations of Toomre & Toomre (1972) to more modern works by Barnes, Hernquist, and others (Barnes & Hernquist 1992, and references therein) it has become apparent that interactions and mergers between galaxies can radically alter their morphology by inducing shells, bars, tails, and other tidal features. Perhaps more importantly, cancellation of angular momentum during the merger process can lead to a radical redistribution of the gas content of the galaxies, with very rapid gas inflow into the galaxy cores. This supply of fresh material could possibly fuel an active galactic nucleus, or provide the high gas densities needed to lead to a sudden burst of star formation.

There is considerable evidence that enhanced star formation is associated with interacting galaxies (Sulentic 1988, and references therein). The young OB stars that dominate the starburst radiate primarily in the optical and ultraviolet, but surrounding gas and dust reprocesses this radiation and thus strongly radiates at thermal wavelengths in the far-infrared. Far-infrared luminosity is thus indicative of the magnitude of recent star formation activity (Telesco 1988; Lonsdale et al. 1984). Additionally, due to the increased temperature of the heated dust, we expect the far-infrared colors to be a good diagnostic of enhanced star formation. Therefore, many studies have therefore concentrated on the far-infrared properties of interacting galaxies.

Several studies have also discussed the incidence of multiple bright galaxies being found within a given interacting galaxy system. Haynes & Herter (1988) found that for galaxy pairs separated by  $2\text{--}10'$ , approximately 10% have multiple components brighter than 0.5 Jy at  $60\mu\text{m}$  and 1 Jy at  $100\mu\text{m}$ . Xu & Sulentic (1991) also concluded that in the majority of interacting systems, only one galaxy is infrared bright. These results agree with an earlier work by Joseph et al. (1984) which concluded, based on near-IR colors, that most often only one galaxy in a pair showed signs of unusual activity. This is an interesting result, because it suggests that specific properties of the interacting galaxies may determine whether or not they become emitters in the far-IR as well. Testing this hypothesis requires resolution of the individual galaxies in the far-IR, which is the goal of this IRAS study.

The canonical figure used by many authors to delineate interacting versus non-interacting systems is a projected separation of three average galactic diameters, as presumably galaxies this close to one another are also close enough to exert a considerable gravitational effect (Dahari 1984; Byrd et al. 1987; Surace et al. 1993). However, for most galaxies detected by IRAS this typically corresponds to an angular separation of a few arcminutes. This is less than the resolution normally achieved by IRAS using the 1-d coadders ADDSCAN or the 2-d FRESCO imaging process. As a result, it has been impossible to study the far-infrared properties of the individual galaxies, and most studies have either made assumptions about the distribution of flux

between galaxies within the interacting system (Bushouse 1986a) or have concentrated on widely separated pairs (Haynes & Herter 1988; Xu & Sulentic 1991). Since previous studies of very widely separated galaxy pairs indicate that in a substantial fraction of interacting systems only one galaxy is unusually active in the far-IR (Xu & Sulentic 1991), it is necessary to resolve these galaxies in order to properly study those properties such as morphology which are unique to the individual galaxies. Additionally, Xu & Sulentic (1991) found evidence that at smaller separations (and hence greater interaction strengths) there was a greater enhancement of far-IR activity. Therefore it would be valuable if these studies could be extended to smaller separations where more observable changes are taking place.

Development of the Maximum Correlation Method algorithm (MCM, Aumann et al. 1990) for use in IRAS image reconstruction significantly increased the resolution of IRAS observations. As implemented in the HIRES process, MCM is an iterative image reconstruction technique that involves using the known response functions of the IRAS detectors to scan simulated image estimates which are then compared to the actual detector data. In this way, a high resolution image estimate is formed. The result is typically a five-fold increase in resolution, varying from roughly  $30'' \times 45''$  at  $12\mu\text{m}$  to  $72'' \times 130''$  at  $100\mu\text{m}$ , with the actual achieved resolution being highly dependent on the geometry of the detector coverage (Surace et al. 1993). Unfortunately, the HIRES process is extremely computer intensive. When developed, a single field typically took a day or more to process. As a result, the earlier work by Surace et al. (1993) was rather limited in scope, with only 23 systems being resolvable. On a modern computer, this computing time is reduced to approximately 15 minutes, thus making feasible the processing of a substantially larger sample <sup>1</sup>.

In Section 2 of this paper we present the sample selection criteria for the objects examined here, and present the data reduction techniques used for reconstructing the IRAS images and measuring the galaxy fluxes. The fluxes at each *IRAS* wavelength are presented in tabular form, and contours of the infrared emission are shown overlaid on optical images of the galaxies. Section 3 presents properties of the catalog, and some results derived from them. Appendix A presents additional notes for selected galaxy systems. Finally, in Appendix B we include data for galaxy systems that were originally included in the RBGS, but were subsequently dropped from the RBGS after a reanalysis of their fluxes. These objects are provided for the interest of the reader, but do not bear on the analysis of the catalog.

## 2. Data

### 2.1. Sample

All of the targets were selected from the IRAS Revised Bright Galaxy Sample (Sanders et al. 2003). The RBGS consists of all 629 galaxies detected by IRAS having a  $60\mu\text{m}$  flux density greater than 5.24 Jy, and is thus similar to and includes all of the well-studied Bright Galaxy Sample (Soifer, Boehmer, Neugebauer, & Sanders 1989), but extends coverage to the entire sky at Galactic latitudes  $|b| > 5^\circ$ .

The following criterion was applied in order to select close pairs from the RBGS:

---

<sup>1</sup>HIRES processing is available from the Infrared Processing and Analysis Center Infrared Science Archive, Jet Propulsion Laboratory, California Institute of Technology [http://irsa.ipac.caltech.edu/IRASdocs/hires\\_over.html](http://irsa.ipac.caltech.edu/IRASdocs/hires_over.html)

$$\frac{2S_{12}}{D_1 + D_2} \leq 3 \quad (1)$$

where  $S_{12}$  is the distance between galaxy centers and  $D_1$  and  $D_2$  are their optical diameters, as measured from the Palomar Sky Survey. This criterion therefore selects all systems where the galaxies are separated by less than three times their average diameter. Note that this excludes very advanced mergers such as Arp 220, where the individual galactic disks can no longer be distinguished. This also has the additional benefit of selecting systems that are sufficiently separated as to be resolvable with HIRES. As such, the sample includes all of the galaxies listed in Table 1 of Surace et al. (1993). Additionally, in an attempt to resolve sources listed in the RBGS which were likely to be confused due to small separations, we included all small galaxy pairs with apparent separation less than  $4'$ . This separation was determined by the normal survey resolution of  $4'$ , which in turn is set by the IRAS  $100\mu\text{m}$  detector size.

## 2.2. Data Reduction

The IRAS data were processed in a manner similar to Surace et al. (1993). The raw detector scans were initially extracted from the IRAS database using the SNIPSCAN process. These raw detector scans were then flattened using an iterative fitting technique that removed the detector baselines, and they were then deglitched in order to remove artifacts such as cosmic ray hits using the LAUNDR process. The HIRES process was then applied to the detector scans. Restoration was done on  $1\Box^\circ$  fields in order to improve detector baseline coverage, with a pixel size of  $15''\text{pixel}^{-1}$ , which is sufficient to adequately sample the restored IRAS beam. The algorithm was iterated 20 times as further iterations tend only to increase noise amplification with little improvement in resolution.

In order to aid in the interpretation of the IRAS data, optical images were extracted from the Digital Sky Survey (DSS) and the IRAS data were overlaid on them (Figure 1). This was valuable in interpreting the correspondence between the resolved IRAS objects and the optical galaxies. In some cases there were small, uncataloged optical galaxies in the DSS images, and the DSS images were used to derive their positions. The optical images have a pixel size of  $1.7''$ . The astrometry of the optical images is based on a linear approximation to the polynomial plate solution provided by STScI, and yields positions accurate to roughly  $2''$  (Laidler et al. 1994). The astrometry of the IRAS images is limited by the pointing accuracy of the satellite, which was approximately  $2''$  in the in-scan direction and  $10''$  cross-scan (Beichmann et al. 1988). Furthermore, the astrometry of point-like sources produced by the HIRES technique is known observationally to be approximately  $20''$  (Laughlin et al. 1990). Thus, registration of the images should be accurate to within one or two HIRES pixel elements, and certainly should be better than the typical IRAS beam size. Optical identifications were made using the coordinates and names given in the NASA/IPAC Extragalactic Database (NED), which are in turn derived from the Third Reference Catalogue of Bright Galaxies (RC3, de Vaucouleurs et al. 1991). When no identifications were available, the galaxies were identified directly from the DSS images and are labeled from northeast to southwest.

Photometry was accomplished in two ways. When the galaxies were cleanly separated, aperture photometry was performed via the IPAC-Skyview software using polygonal apertures of a size sufficient to insure that all of the galaxy flux was measured. In those cases where components appeared to be resolved but not separated, the data were modeled with 2-d elliptical Gaussians using the AIPS IMFIT and JMFIT routines. This is justified in that although the geometry of the IRAS beam is variable, it usually has roughly the

form of an elliptical Gaussian whose exact size and orientation depend on the detector scan geometry. Peak positions were constrained to the position indicated by the nearest separated IRAS wavelength. If none of the IRAS data were able to supply positions, then the Gaussian centers were constrained to the locations of the optical peaks as given by the RC3, where possible, and otherwise according to positions measured directly from the DSS. Note that the latter could introduce a bias in that it presupposes correspond between the infrared and optical centers. In cases where the galaxies are well-separated at optical wavelengths, the optical and infrared peaks do correspond. Many of the galaxies that were decomposed using gaussian fitting are also well-separated at optical wavelengths, but are too close to one another to be separated by IRAS. In these cases it is reasonable to assume that the optical peaks will correspond to the infrared peaks. Only in cases of advanced mergers, such as NGC 4038, would this assumption break down.

Table 1 presents the measured global photometry for each of the galaxies identified in the IRAS images from the RBGS sample. The supporting data in Table 1 and Table 2 were taken from the NED, and relevant notes regarding this database are given below. It should be noted that the magnitudes, morphological types, etc. listed by NED are generally not on any homogeneous system, although when possible data from NED is derived from the RC3. The table is ordered by increasing B1950 Right Ascension of the galaxy systems, as given by the western-most component. The columns are as follows:

Column 1 - The galaxy name. Names are given in order of preference from the NGC, UGC, Catalog of Galaxies and Clusters of Galaxies (CGCG), Morphological Catalogue of Galaxies (MCG), Markarian (Mrk), and 2MASS catalogs. Relevant cross-id's are also given. The given names are those associated with a specific coordinate as given by the RC3, NED, or the Arp atlas. The Arp name associated with a given galaxy group is listed with the first (westernmost) object, but no special significance is indicated by this.

Column 2,3 - Equinox 1950 coordinates. The given coordinates are those of the centroid of the infrared emission in cases where there was a separated infrared detection. Otherwise, the optical position from NED is listed. In almost all cases these coordinates originate from the RC3, although currently NED lists values from the Two Micron All Sky Survey (2MASS). If NED listed no coordinates, then the coordinates are those measured directly from the DSS. Equinox B1950 coordinates were chosen because this is the epoch of the positional calibration for the IRAS Level 1 Archive scans used to construct the HIRES images.

Column 4 - The position type. If “O”, then the given position is an optical center, and if “I” then a new infrared center derived from the HIRES images.

Column 5 - Radial velocity in  $\text{km} \cdot \text{s}^{-1}$ . In all cases where these are listed they are spectroscopic redshifts from a variety of sources as given by NED. Uncertainties are typically 10-100 km/sec.

Column 6 - Total optical magnitude as given by NED. In most cases this is the blue magnitude listed in the RC3.

Column 7-14 - 12, 25, 60, and 100  $\mu\text{m}$  integrated fluxes in Jy, and the associated  $1-\sigma$  uncertainties. In cases where the targets were also given by Surace et al. (1993), the objects were remeasured in order to ensure uniformity of calibration with the rest of the survey (see Section 2.3). In some cases the galaxies were still unresolved at all wavelengths. In this case only the global flux, as measured from the HIRES data, is given. In cases where one or more components remained unresolved, but some components were resolved, the brightest unresolved component in the resolved waveband gives the flux of all the components, and subsequent unresolved components are marked with ellipses. Upper limits are denoted with a “<” and are the flux measured at the known optical location of the galaxy in an aperture that has the same size as the effective IRAS beam.

Column 15 - Log of the far-infrared luminosity, in units of solar luminosities. This is the luminosity from 40–122 $\mu$ m (Helou et al. 1988).  $H_0 = 75 \text{ km s}^{-1} \text{ mpc}^{-1}$  is assumed. This quantity is useful for photometric study, is not very sensitive to the shape of the spectral energy distribution, and is the quantity tabulated by Surace et al. (1993). The  $L_{fir}$  described in the RBGS is the luminosity from 1–500 $\mu$ m. It was derived by applying a correction factor to the flux between 40–122 $\mu$ m based on the 60/100 $\mu$ m color (Lonsdale et al. 1985). For the galaxies described here, the median correction factor is  $1.44 \pm 0.09$ . In other words,  $\text{Log } L_{1-500\mu m} = \text{Log } L_{40-122\mu m} + 0.16$ . This is also different from the quantity  $L_{ir}$  as described by Sanders & Mirabel (1996), which is the flux from 8–1000 $\mu$ m, but which generally cannot be computed here since it requires detections in all four IRAS bands.

### 2.3. Photometric Uncertainties

Evaluating the photometric uncertainty of the HIRES data product is quite difficult. In general, uncertainties arise from three sources, all of which vary in importance depending on the particular field. The integrated flux density uncertainties quoted in Tables 1 & 2 contain measurement and confusion errors, but *not* systematic effects in the overall calibration.

Confusion is the first limitation. The dominant source of noise in HIRES is not photometric background noise, but confusion due to noise spike amplification. High sigma noise peaks are amplified by the deconvolution process; they appear similar to weak point sources with a signal strength as high as 0.1 Jy. These spikes are illustrated in Figure 2. This results in a highly non-Gaussian single-sided noise distribution on spatial scales similar to the beam size, not the pixel size. In those cases where the galaxy fluxes are less than 0.3 Jy, it becomes difficult to differentiate the target from amplified noise. As a result, quoted upper limits are often quite high, as this upper limit is set by the flux contained in these noise peaks. Our achieved sensitivity is thus around 0.25–0.3 Jy, depending on the wavelength and field geometry. Similarly quoted uncertainties are often also high, depending on the amplitude of these spikes. Apertures similar to the effective beam size were used to evaluate a median false signal due to the noise spikes. These spikes are the dominant source of uncertainty for faint objects.

The technique used to derive the photometry is the second contributor to the photometric uncertainty. In cases where the galaxies are well separated and aperture photometry could be used, this typically contributes only a few percent to the total error. In those cases where the galaxies were not well separated and Gaussian fitting was used, this becomes the dominant source of error and can range anywhere from 20–50% depending on the degree of resolution of the targets.

Absolute photometric calibration is the third major source of uncertainty, and which is not included in Table 1. As noted in Surace et al. (1993), there are certain caveats to the photometric calibration of the HIRES data product. In particular, the calibration of the IRAS data is in part dependent on factors due to detector responsivity and dwell time. Known as the AC/DC correction, it is the difference in responsivity for point sources versus extremely extended sources, which was characterized as a function of detector dwell time based on the nominal survey slew speed. This is well known for point sources, and hence the Point Source Catalog (PSC) is properly calibrated (Beichmann et al. 1988). However, it is slightly different for small extended sources, and is a poorly understood function of source extension. This was seen during the data analysis presented in Paper I, where it was found that the majority of the HIRES fluxes were significantly greater than the values estimated using one-dimensional coaddition with the ADDSCAN/SCANPI processing available at IPAC. In Paper I this issue was wholly avoided by forcing all of the data onto the same flux

scale as the PSC by using the component flux ratios indicated by HIRES to divide up the flux indicated by the BGS, which was produced using the ADDSCAN process which is known to have the same photometric scale as the PSC.

Figure 3 through 6 show the difference in flux estimates between this paper and the ADDSCAN/SCANPI values published in the RBGS (Sanders et al. 2003). The data points shown in these figures are limited to cases where the flux referred to in the RBGS was unambiguous. These are primarily systems which were either unresolved by HIRES (and hence both catalogs have single fluxes) or were sufficiently separated as to have been resolved by both ADDSCAN/SCANPI and HIRES (e.g. NGC 875). The mean offsets between the two catalogs are 27.5, 12.8, 4.5, and 5.5 % at 12, 25, 60, and 100  $\mu\text{m}$ . The observed scatter around the mean is similar to the estimated flux uncertainties in Table 1. These are particularly significant in the faint 12 $\mu\text{m}$  channel, where although the minimum requirement for reporting is a  $S/N > 3$ , the average detection only has a  $S/N \approx 5$ . The mean offsets are also similar in size to the observed scatter. Testing of HIRES has shown that measured integrated fluxes of unresolved point sources have an intrinsic scatter of about 8-12% compared to those of the PSC (Laughlin et al. 1990). In all cases the one sigma scatter in offsets observed for the galaxies is larger than the value of the systematic offset. There is no statistically significant trend as a function of flux. In several cases the statistically significant outliers seen in the brighter channels are a result of differences in background estimation between the one-dimensional ADDSCAN results and the two-dimensional HIRES results.

While the version of HIRES used in this paper produces data believed to be on the AC scale, appropriate for point sources, it is clear that there are systematic offsets relative to other AC-calibrated IRAS data products. Previous experiments in Paper I showed that the HIRES data product correctly reproduces the photometry of point sources in accordance with the PSC. As the exact source of this offset remains unclear, as does the calibration for small extended sources, this data has not been forced to agree with the RBGS, unlike Surace et al. (1993). This is the source of the variations between the fluxes in Paper I and this work.

As a result of this offset, the results presented here differ from those based solely on PSC-calibrated products by small amounts. The ratio of 60 to 100 $\mu\text{m}$  flux remains unchanged, as the offset is the same in both bands. The infrared luminosities are 5% higher, a value considerably less than the typical uncertainty. The log of the 12 to 24 $\mu\text{m}$  ratio differs by being 0.05 higher. When appropriate, these offsets will be discussed in the Section 3 of this paper.

### 3. Results

#### 3.1. Far-IR Properties

The cumulative distribution functions (CDFs) of  $L_{\text{fir}}$ ,  $\text{Log}(f_{12}/f_{25})$ , and  $\text{Log}(f_{60}/f_{100})$  are given in Figures 7, 8, and 9. These distributions only include the galaxies actually detected and resolved by HIRES. These distributions are nearly identical to Surace et al. (1993). This is to be expected, since the shape of the CDF remains unchanged so long as the nature of the incompleteness in the data is random. Since Paper I differed from this paper in being drawn from a parent sample which was different from the RBGS primarily in spatial extent on the sky, the CDFs are expected to remain the same.

As in Surace et al. (1993), a comparison sample of galaxies was constructed by selecting a subsample drawn from the BGS which had no visible signs of interaction and were not in close pairs (this is the same sample described in Paper I). From these isolated BGS galaxies we selected a subsample so as to have the

same distribution of blue magnitudes as the RBGS close pairs. We can therefore compare the far-infrared properties of a far-infrared flux-limited sample of interacting pairs to a similarly flux-limited sample of isolated galaxies with the same distribution of optical luminosities.

The CDF for  $\text{Log } L_{\text{fir}}$ , which is computed from the 60 and  $100\mu\text{m}$  fluxes, is shown in Figure 7. The median value of  $L_{\text{fir}}$  is  $10^{10.50} L_{\odot}$  for individual, resolved galaxies in the paired and multiple RBGS systems studied here. This is somewhat higher than found in Paper I ( $L_{\text{fir}}=10^{10.30} L_{\odot}$ ), and cannot be readily attributed to the offsets in calibration, which are of order 5% at these wavelengths. Kolmogorov-Smirnov statistics indicate that the isolated and paired samples are not drawn from the same parent sample at better than the 99.99% confidence level. In separated galaxy pairs, then, the interaction process enhances  $L_{\text{fir}}$  by a factor of roughly 3.

Similar differences are seen in the far-IR colors. The median value of  $\text{Log}(f_{12}/f_{25})$  is -0.36 for resolved component galaxies in pairs vs -0.19 for isolated galaxies. Paper I found -0.43 and -0.2. However, as noted earlier, this may be a result of the differing flux calibration between Paper I and this paper. Adjusting for this produces a mean  $\text{Log}(f_{12}/f_{25})$  of -0.41 for individual galaxies in the RBGS HIRES interacting galaxy sample. The maximum difference in the CDF is 0.31 and occurs at  $\text{Log}(f_{12}/f_{25}) = -0.28$ . Kolmogorov-Smirnov statistics reject the null hypothesis that these two sample are drawn from the same parent sample at better than the 99.99% level.

A median  $\text{Log}(f_{60}/f_{100})$  value of -0.25 is observed for galaxies belonging to pairs and groups in the RBGS HIRES sample, compared to -0.34 for non-interacting RBGS galaxies. This is the same result as seen in Paper I. The difference in CDF between the two samples is less pronounced overall than at the shorter wavelengths. Nevertheless the maximum difference in CDFs is 0.34 at  $\text{Log}(f_{60}/f_{100})=-0.29$ . Again, we can reject the null hypothesis that the two samples were drawn from the same sample at better than the 99.99% level.

### 3.2. Pairing in the Far-IR

While there is clearly evidence that pairs and groups of galaxies generally have higher star formation activity compared to isolated galaxies, there is still uncertainty regarding the relative degree to which enhanced star formation is triggered in individual galaxies during various phases of the interaction and merger process. Naively, among spiral-spiral pairs that have companions with nearly equal B-band luminosities, one would expect that both galaxies contribute in similar proportions to the total far-infrared emission of the pair. Previous authors, as discussed earlier, have generally concluded that for very distant pairs observed in the far-IR only one galaxy is infrared active. Other authors, working at optical and near-IR wavelengths, have reached the same conclusion using indirect measures of star formation. Using the higher resolution images presented here, it is possible to test this result over a much wider range and smaller absolute separations than previously possible. Figure 10 plots the measured flux ratios (solid circles) and upper limits (open circles) at the longest resolvable wavelength between the brightest galaxy and its companion as a function of the total far-infrared luminosity,  $L_{\text{fir}}$ . For galaxy groups, the ratio plotted is the flux of the brightest galaxy divided by the average flux of the companion galaxies in the group. These results provide little evidence that both companions contribute comparably to the infrared emission, and that there is no increased tendency for infrared luminous galaxies to be found with other infrared luminous galaxies. That is, 66% of the interacting systems have component flux ratios greater than 3, 56% have ratios above 5, and 36% have ratios greater than 10. Surace et al. (1993) claimed that in approximately 2/3 of interacting pairs,



the ratio of the flux densities of the companions are less than 10, which is confirmed here in the much larger sample of infrared-bright galaxy system investigated here.

Figure 10 also shows that over the range of  $L_{\text{fir}}$  spanned by this RBGS subsample, there is no clear correlation between the companion galaxy flux ratios and  $L_{\text{fir}}$ . Although at flux levels  $\text{Log}(L_{\text{fir}}/L_{\odot}) > 11$  there suggestively are almost no systems where the component flux ratio is less than three, our sample does not extend to such high luminosities as would produce a clearer result. This is because our selection criteria biases us against very advanced mergers, which are the majority of the luminous and ultraluminous infrared galaxies. Since both components in an interacting system are presumably undergoing a similar degree of tidal disruption, it seems that in the relatively early stages of interaction sampled here, the details of the encounter itself are less important than characteristics of the individual galaxies in determining the degree of far-infrared enhancement. Major factors expected to play an important role are the molecular gas content available to fuel star formation and the mass of the stellar bulge which may regulate the degree of accretion onto a supermassive black hole.

Finally, we can examine whether or not confusion has caused galaxies to be erroneously included in the RBGS because their combined flux was high enough to meet the flux limit criterion, but which would not have been selected if they could be resolved. Figure 11 presents the cumulative distribution functions of  $60\mu\text{m}$  fluxes for the HIRES-resolved galaxies above and below the 5 Jy selection limit. An examination of Table 1 shows that there are 2 systems that appeared in the RBGS by virtue of having a combined, unresolved flux above the 5.24 Jy limit at  $60\mu\text{m}$  but whose individual components were all clearly below this limit (IC563/4, NGC 7752/3). An additional five (IC 2522/3, UGC 6436a/b, NGC 3991/4/5, MCG -03-34-063a/b, and VV 414) have only one component whose flux including uncertainties may be as high as the RBGS flux limit. Thus, close pairs in the RBGS verifiably affect the selection of the sample at only the 0.3% level (2/629), and at worst may account for 1.1%. This statement applies to separated pairs resolved by HIRES in this study. Very close pairs with separations less than  $\approx 30''$  (typically ongoing mergers in the local Universe) which cannot be resolved by HIRES account for increasingly larger fractions of RBGS objects as a function of increasing total far-IR luminosity (e.g., see review by Sanders & Mirabel 1996). The manner in which the total far-IR fluxes of such objects are distributed between the individual components remains unknown for such pairs, and these will be fruitful targets to study with higher resolution using observatories such as SIRTf and SOFIA.

### 3.3. Optical Morphology and far-IR Enhancement

Recent computational models by Mihos & Hernquist (1994a,b) have predicted that the presence of a large central bulge in a galaxy will help stabilize it against tidal perturbation. Specifically, they found that in major mergers of galaxies the presence of a central bulge inhibits the flow of gas into the central few kiloparsecs of a galaxy, thus preventing high gas densities from being quickly reached and suppressing any period of rapid star formation until the end of the merger (Mihos & Hernquist 1994b). Thus, late-type spirals are expected to experience starbursts during the initial stages of merger, while early-type spirals undergo strong starburst activity only during the completion of the merger process. This provides a mechanism to delay the onset of starburst activity in some systems until very advanced merger stages are reached, as otherwise it is difficult to invoke a starburst model for ultraluminous infrared galaxies (which appear to be very advanced mergers) given the expected timescale for starbursts. Since very evolved mergers have such disturbed morphologies that it is difficult to determine the form of the merger progenitors, the most viable observational test is to examine young merger systems which have not evolved as far away from their original

forms and look for evidence for the onset of enhanced far-IR activity in bulgeless galaxies.

Hubble types were taken from NED. A fraction of the galaxies either have not been classified at all, or are simply listed with generic types such as “spiral”. All other resolved spiral galaxies that were actually classified were considered to be either “early type” (S0, SB0 through Sa, SBa) or “late-type” (Sb,SBb and higher). Although the specific Hubble type for each galaxy was kept track of, for purposes of this analysis it was felt to be more useful to group the types into such very broad categories in order to improve the counting statistics.

Only 11 ellipticals known from optical imaging of the galaxy pairs are found in the entire sample. Of these, none are detected at both 60 and 100 $\mu$ m and only three are detected by IRAS at any wavelength. These numbers agree with what would be expected based on a random pairing of elliptical and spiral galaxies given an elliptical/spiral fraction similar to that of field galaxies, or are perhaps a little low. In particular, this is the number expected if we assume that every system contains one bright spiral galaxy, and that the remaining faint galaxies are distributed according to the field elliptical/spiral ratio. This also agrees with the low detection fractions for elliptical galaxies found by other studies (Sulentic 1988; Haynes & Herter 1988).

An examination of the late and early-type spirals in the sample indicates that there are no differences between these populations. The rate of detection for both of the two classes is around 88%, indicating that they have a similar fraction of their distribution above our detection limit. This is further illustrated by Figure 12, which shows the cumulative distribution function of  $\text{Log } L_{\text{fir}}$  for the galaxies which were actually detected in the two classes. They are extremely similar. The K-S test cannot reject the null hypothesis that the two samples are drawn from the same sample with better than 65% confidence. Results are the same for the color ratios  $\text{Log}(f_{12}/f_{25})$  and  $\text{Log}(f_{60}/f_{100})$ .

Similar results also hold for different combinations of Hubble sub-types, such as considering only S0 galaxies as “early”. Haynes & Herter (1988) found that the detection rate for isolated spiral galaxies is roughly independent of morphological type. Roberts & Haynes (1994) have confirmed this using large optical samples of isolated galaxies and comparing them against the IRAS data. The median, 25% and 75% percentile values of the distribution of  $L_{\text{fir}}$  for the sample spiral galaxies are also very similar to those found by Roberts & Haynes for isolated UGC galaxies. This is unsurprising, since both the results presented here and previous studies have shown that only a small increase in  $L_{\text{fir}}$  occurs for widely separated (non-overlapping) interacting pairs (Haynes & Herter 1988; Surace et al. 1993), and therefore any enhanced far-IR activity that could distinguish late from early spirals is likely to be slight. This enhancement would be further diluted by the presence of systems that have not yet reached first perigalacticon, and hence have not yet reached the point at which the two classes would separate themselves (Mihos & Hernquist 1994b), and by the presence of systems which are unlikely to actually merge or otherwise strongly interact with each other.

#### 4. Conclusions

We have presented an atlas of high resolution IRAS observations of all 106 of the paired (and in many cases interacting systems) in the IRAS Revised Bright Galaxy Sample with a 60 $\mu$ m flux density greater than 5.24 Jy. The atlas contains infrared contours overlaid on optical images and a catalog of fluxes or upper limits in all four IRAS wavebands.

We have presented the infrared luminosities and colors of the paired galaxy sample, and compared them

to a sample of isolated galaxies. We find substantially the same results as Surace et al. (1993), namely that the paired galaxies have a measurably different distribution of infrared properties than isolated galaxies.

Using morphological optical classifications for the galaxies we conclude that there is no difference between late and early-type spirals in terms of their far-IR properties. In particular, no significant enhancement is seen in the far-infrared luminosity or color of the late-type spirals as compared to the early-type spirals.

We would like to thank Ron Beck and John Fowler for their assistance in setting up our HIRES processing facility, and in particular Diane Engler for her speedy work in extracting the detector scans from the IRAS database. We thank an anonymous referee for his or her comments that led to an improved presentation of these results.

This work has made use of the NASA/IPAC Extragalactic Database (NED) which is operated by the Jet Propulsion Laboratory, California Institute of Technology, under contract with the National Aeronautics and Space Administration. It has also made use of the Digitized Sky Survey, produced at the Space Telescope Science Institute under U.S. Government grant NAG W-2166. This was based on photographic data obtained using the Oschin Schmidt Telescope on Palomar Mountain, operated by the California Institute of Technology, and the UK Schmidt Telescope, which was operated by the Royal Observatory Edinburgh and the Anglo-Australian Observatory. JAS and JMM were supported by the Jet Propulsion Laboratory, California Institute of Technology, under contract with NASA. DBS acknowledges support from a Senior Award from the Alexander von Humboldt Foundation and from the Max-Planck-Institut für extraterrestrische Physik as well as support from NASA grant NAG 90-1217.

### A. Notes on Individual Galaxy Systems

*NGC 520* — the flux in this advanced merger appears to be centered between the two galaxies, in what appears to be a dust lane.

*IC 2163* — this system is somewhat puzzling in that there is significant emission to the west of the center of the western galaxy in the pair. Additionally, in general the peak flux appears to occur between the galaxies. It is notable that the reconstructed *IRAS* beam is unfortunately elongated at nearly the same position angle as the two galaxies, and hence the irregular beam is confusing the location of the emission.

*NGC 4038/9* — the emission originates between the galaxy centers in the region where the disks overlap. This is consistent with the results of Vigroux et al. (1996).

*IC 4153* — there is a sizable discrepancy between the HIRES flux and the ADDSCAN flux used by the RBGS at 100  $\mu\text{m}$ . Furthermore, the HIRES flux given in Table 1 agrees with the flux indicated by the FRESKO data product. FRESKO is a two-dimensional coadd data product available from IPAC. This coadd is not an iterative reconstructed image, and hence should not suffer from iterative artifact amplification. An examination of the complex structure seen in HIRES and FRESKO images surrounding this source, as well as the details of the ADDSCAN processing, show that this discrepancy is probably due to differences in the baseline (background) fitting.

*NGC 5953/4* — given as CPG 468 by Domingue et al. (2003). The HIRES data agrees with the higher resolution ISOPHOT data indicating the dominance of the southwestern component.

*NGC 6907/8* — the galaxy NGC 6908 is actually a small spiral galaxy superimposed on the NE arm of NGC

6907, and is most clearly seen in near-infrared images. It cannot be resolved by HIRES. This system appears in Appendix B.

*NGC 7752/3* — also known as CPG 591. (Domingue et al. 2003) find that the southwestern component is more peaked and dominates the ISOPHOT 60 and  $100\mu\text{m}$  data. The HIRES data supports this finding, particularly in the mid-IR.

## B. Additional Galaxy Systems

In addition to the 106 galaxy systems detailed in Section 2, several other systems were also processed. During the compilation of the RBGS Sanders et al. (2003), the IRAS data were recalibrated, and the choice of flux measures used to estimate the IRAS fluxes changed. As a result, there are a handful of systems which appear in the BGS<sub>1</sub>+BGS<sub>2</sub> but not the RBGS, and vice versa. These are detailed in the RBGS, Section 3.2. As a result, some additional galaxy systems were processed with HIRES, but do not belong in the RBGS sample proper and were not included in Table 1 of this paper. They are presented here for informational purposes. The images are shown in Figure 13, and the tabulated fluxes appear in Table 2.

## REFERENCES

- Aumann, H.H., Fowler, J.W., & Melnyk, M. 1990. *AJ*, 99, 1674
- Barnes, J. & Henrquist, L. 1992. *ARA&A*, 30, 705
- Beichmann, C.A., Neugebauer, G., Habing, H.J., Clegg, P.E., & Chester, T.J. editors. 1988. *IRAS Catalogs and Atlases, Explanatory Supplement*. (U.S. GPO, Washington, D.C.) IV.
- Bushouse, H.A. 1986a. *AJ*, 91, 255
- Byrd, G.G., Sundelius, B., & Valtonen, M. 1987, *A&A*, 171, 16
- Combes, F., Prugniel, P., Rampazzo, R., & Sulentic, J.W., 1994, *A&A*, 281, 725
- Dahari, O. 1984, *AJ*, 89, 966
- Domigue, D.L., Sulentic, J.W., Xu, C., Mazzarella, J., Gao, Y., & Rampazzo, R. 2003, *AJ*, 125, 555
- Elfhag, T., Booth, R.S., Hoglund, B., Johansson, L., & Sandqvist, A. 1996, *A&A Supp. Ser.*, 115, 439
- Haynes, M.P. & Herter, T., 1988, *AJ*, 96, 504
- Helou, G., Khan, I.R., Malek, L., & Boehmer, L. 1988, *ApJS*, 68, 151
- Joseph, R.D., Meikle, W.P., Robertson, N.A., & Wright, G.S., 1984, *MNRAS*, 209, 111
- Laidler, V.G., Rehner, D.M., & Sturch, C.R. 1994. *The Digitized Sky Survey*, (Space Telescope Science Institute)
- Larson, R.B., & Tinsley, B.M. 1978, *ApJ*, 219, 46
- Laughlin, G., Engler, D., & Rice, W. 1990, *HIRES Product Validation: I. Point Sources*. (Infrared Processing and Analysis Center Memo 701-90-077/2).

- Lonsdale, C.J., Helou, G., Good, J.C., & Rice, W. 1985, Cataloged Galaxies and Quasars Observed in the IRAS Survey, Jet Propulsion Laboratory
- Lonsdale, C.J., Persson, S.E., & Mathews, K. 1984, ApJ, 287, 95
- Mihos, J.C., & Hernquist, L. 1994, ApJ, 425, L13
- Mihos, J.C., & Hernquist, L. 1994b, ApJ, 431, L9
- Roberts, M. & Haynes, M.P. 1994, ARA&A, 32,115
- Sanders, D.B., & Mirabel, I.F., 1996, ARA&A, 34, 749
- Sanders, D. B., Egami, E., Lipari, S., Mirabel, I. F., & Soifer, B. T. 1995, AJ, 110, 1993 (BGS2)
- Sanders, D.B., Mazzarella, J.M., Kim, D-C., & Surace, J.A., 2003, AJ, in press (RBGS)
- Soifer, B. T., Boehmer, L., Neugebauer, G., & Sanders, D. B. 1989, AJ, 98, 766 (BGS)
- Sulentic, J. 1988, AJ, 98, 2066
- Surace, J.A., Mazzarella, J.M, Soifer, B.T., & Wehrle, A.E. 1993, AJ, 105, 864 (Paper I)
- Telesco, C.M. 1988, ARA&A, 26, 343
- Toomre, A., & Toomre, J. 1972, ApJ, 178, 623
- Vigroux, L. et al. 1996, A&A, 315, L93
- Xu, C., Gao, Y., Mazzarella, J., Lu, N., Sulentic, J. W., & Domingue, D. L. 2000, ApJ, 541, 644
- Xu, C. & Sulentic, J. W. 1991, ApJ, 374, 407
- Young, J.S., Schloerb, F.P., Kenney, J.D., & Lord, S.D., 1986, ApJ, 304, 443
- Zink, E.C., Lester, D.F., Doppmann, G., & Harvey, P.M., ApJS, 131, 413

Fig. 1.— HIRES data for each pair or group in the RBGS overlaid on gray-scale images from the Palomar Digital Sky Survey. The contours are at intervals of 10, 16, 25, 40, and 63% of the peak flux; they show the results of 20 iterations of the MCM algorithm, and represent the highest achievable IRAS resolution at 12, 25, 60 and  $100\mu\text{m}$ . The axis labels are B1950 coordinates. The scale bar inside each  $100\mu\text{m}$  panel represents 50 kpc or 25 kpc at the distance of the system (as labeled).

Fig. 2.— Illustration of amplification of high-sigma noise outliers by the HIRES process, resulting in noise “spikes” similar in size to the reconstructed IRAS beam and having total fluxes of  $\approx 0.1$  Jy. This is the  $60\mu\text{m}$  image of Arp 271.

Fig. 3.— Fractional difference between one-dimensional ADDSCAN/SCANPI fluxes (Sanders et al. 2003) and HIRES fluxes at  $12\mu\text{m}$ . The horizontal axis is the RBGS flux in Jy. The vertical axis scaling is such that 0.2 indicates a difference of 20%.

Fig. 4.— Same as Figure 3, but for  $25\mu\text{m}$ .

Fig. 5.— Same as Figure 3, but for  $60\mu\text{m}$ .

Fig. 6.— Same as Figure 3, but for  $100\mu\text{m}$ .

Fig. 7.—  $L_{\text{fir}}$  cumulative distribution function for single, isolated galaxies in the RBGS and individual galaxies in multiple systems resolved by HIRES. The resolved individual galaxies in RBGS paired systems show a small ( $\approx 3\times$ ) increase in  $L_{\text{fir}}$  compared to isolated galaxies

Fig. 8.— CDFs of  $\text{Log}(f_{12}/f_{25})$  for paired and isolated galaxies, as in Figure 7.

Fig. 9.— CDFs of  $\text{Log}(f_{60}/f_{100})$  for paired and isolated galaxies, as in Figure 7.

Fig. 10.—  $\text{Log } L_{\text{fir}}$  versus the pair component flux ratio. Closed circles are measured ratios, while open circles are upper limits. No correlation is seen. The distribution of lower limits is somewhat random, since there was a fixed lower flux limit for the dim component, while the bright component could span a wide range of detected brightnesses.

Fig. 11.— Integrated, spatially resolved  $60\mu\text{m}$  flux cumulative distribution functions for galaxies detected in the RBGS.

Fig. 12.— Cumulative distribution function of  $L_{\text{fir}}$  of late and early-type interacting spiral galaxies in the RBGS. There is no measurable difference between the two.

Fig. 13.— HIRES data as in Figure 1 for additional galaxy systems processed but not members of the final RBGS, as described in Appendix B.

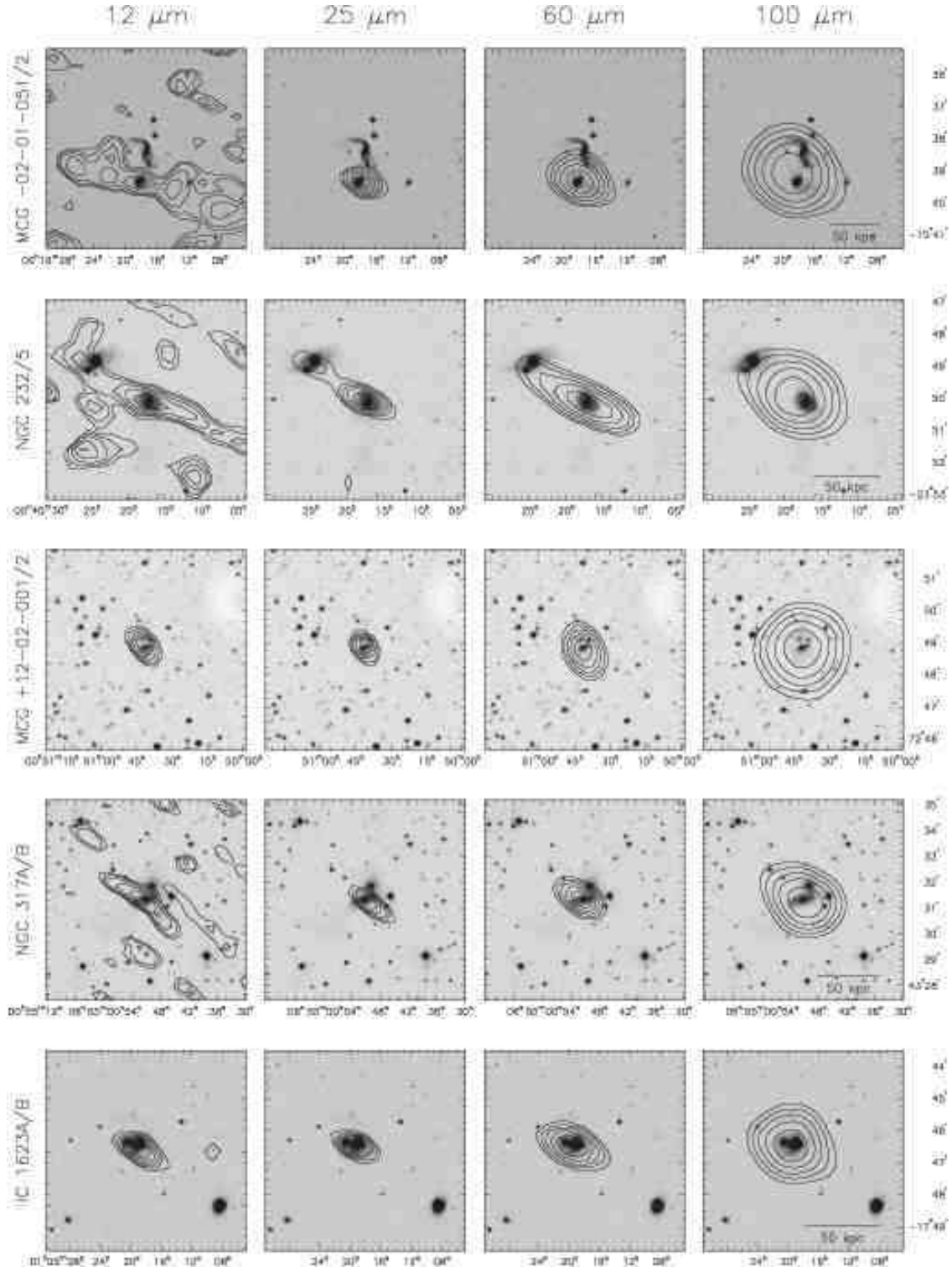


Fig. 14.—

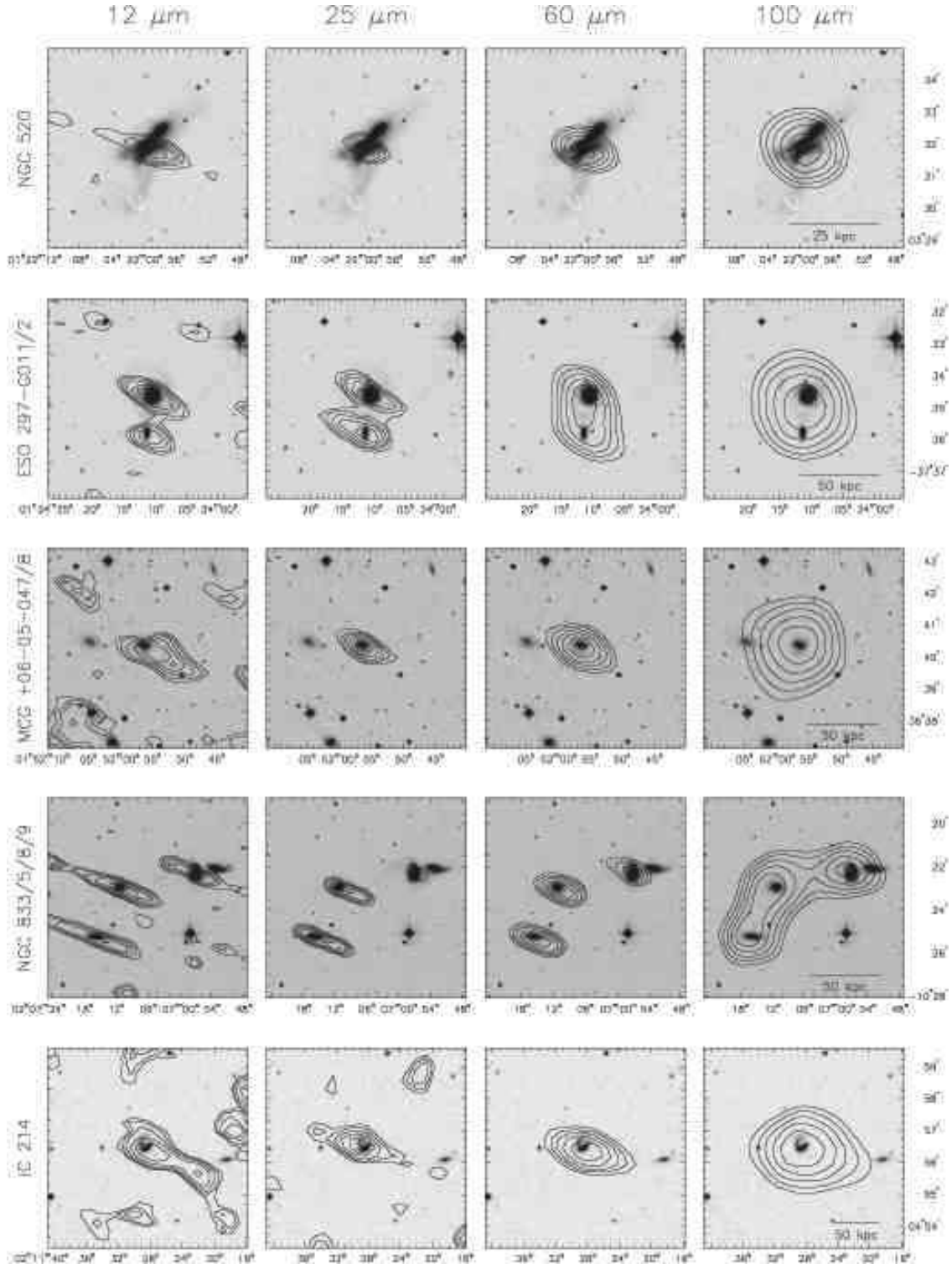


Fig. 1 cont.—



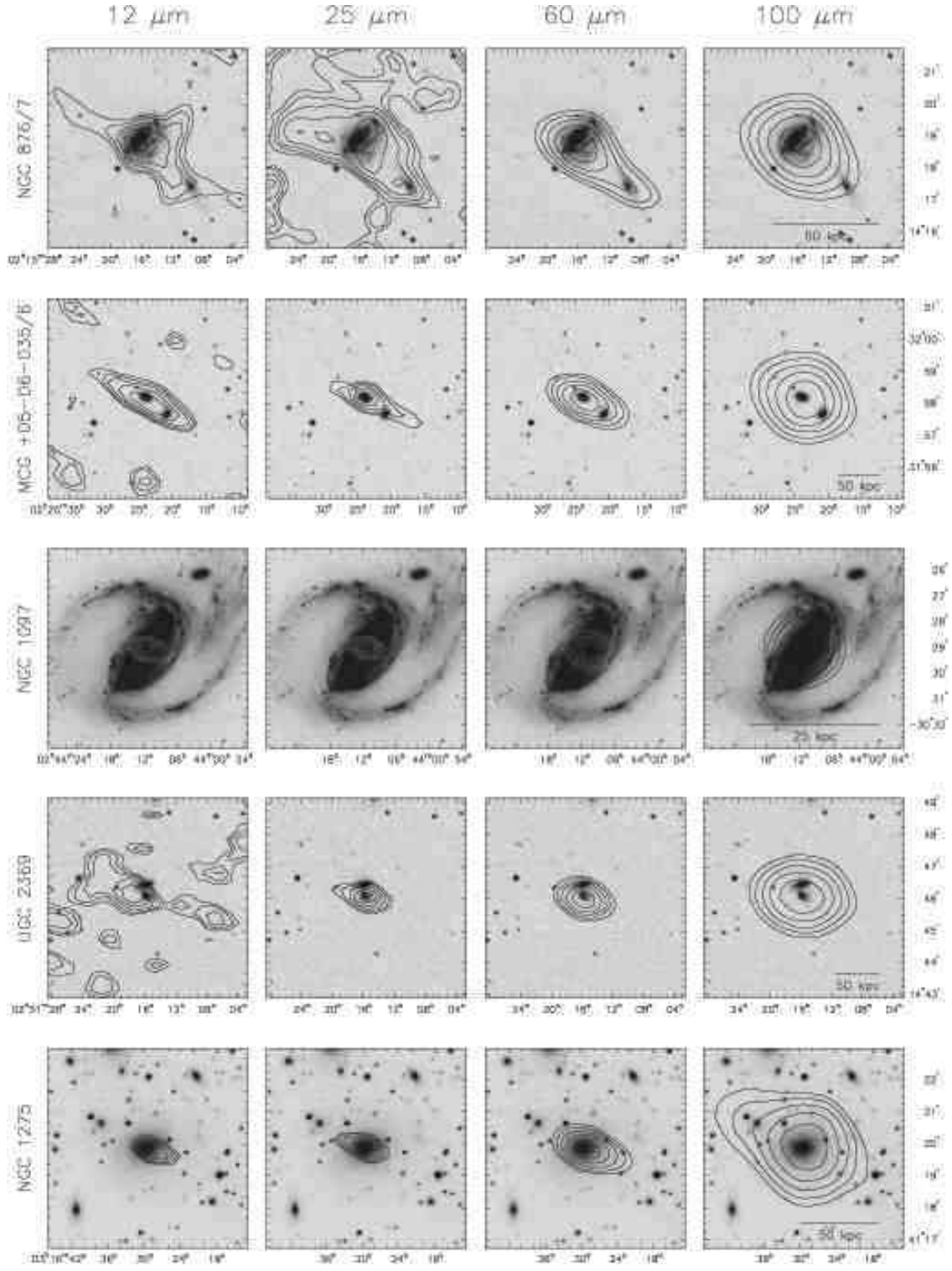


Fig. 1 cont.—

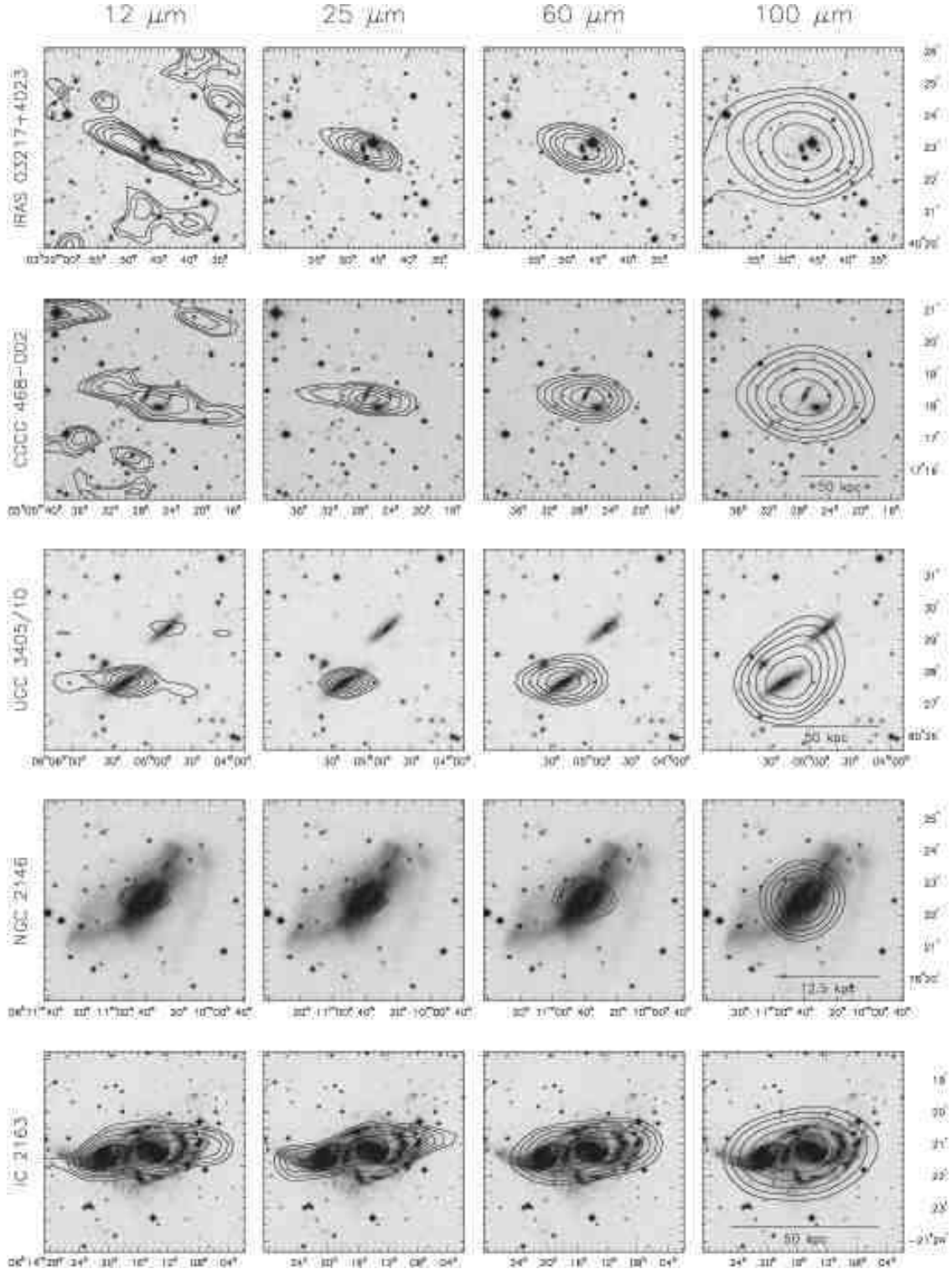


Fig. 1 cont.—

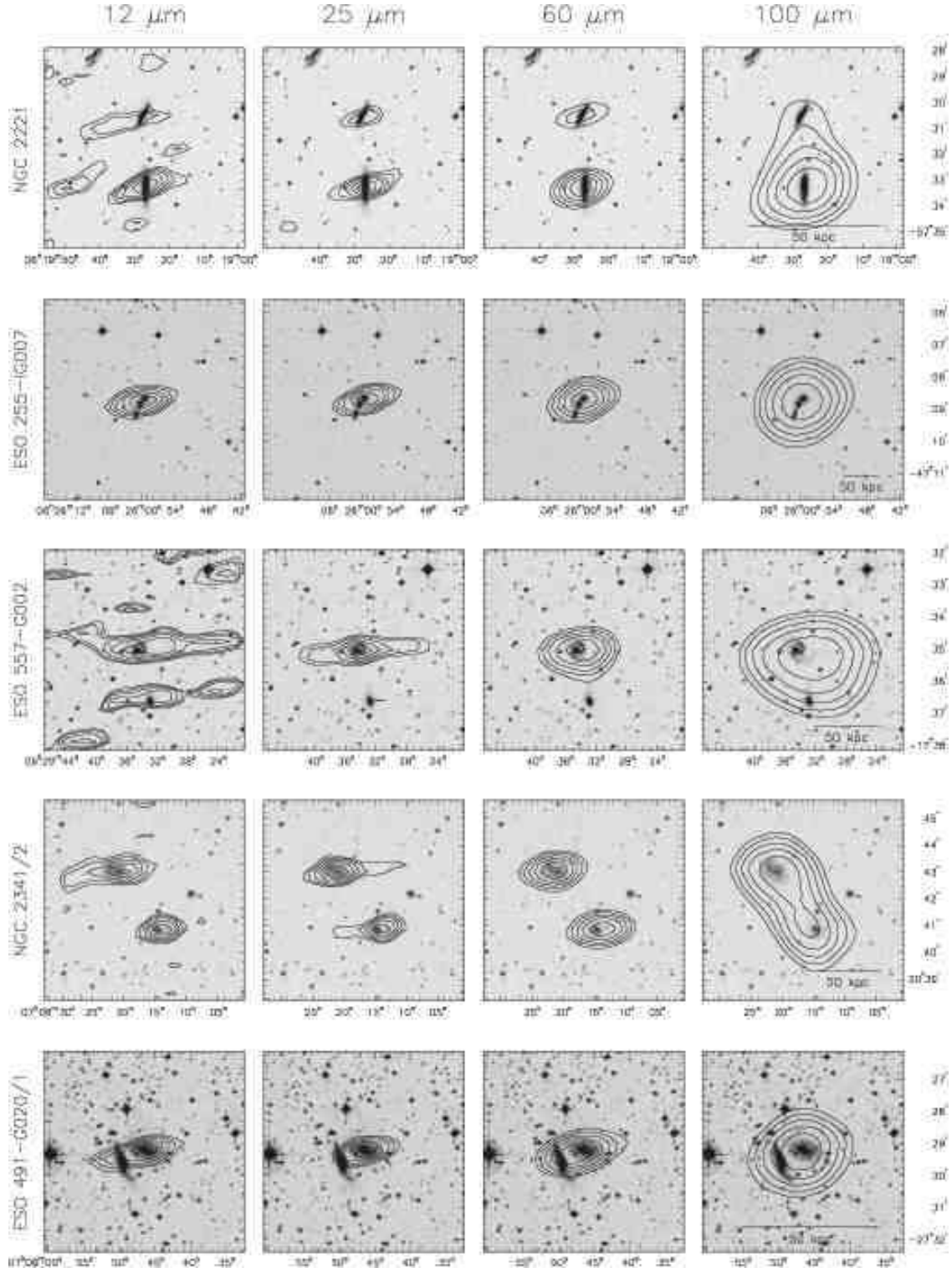


Fig. 1 cont.—

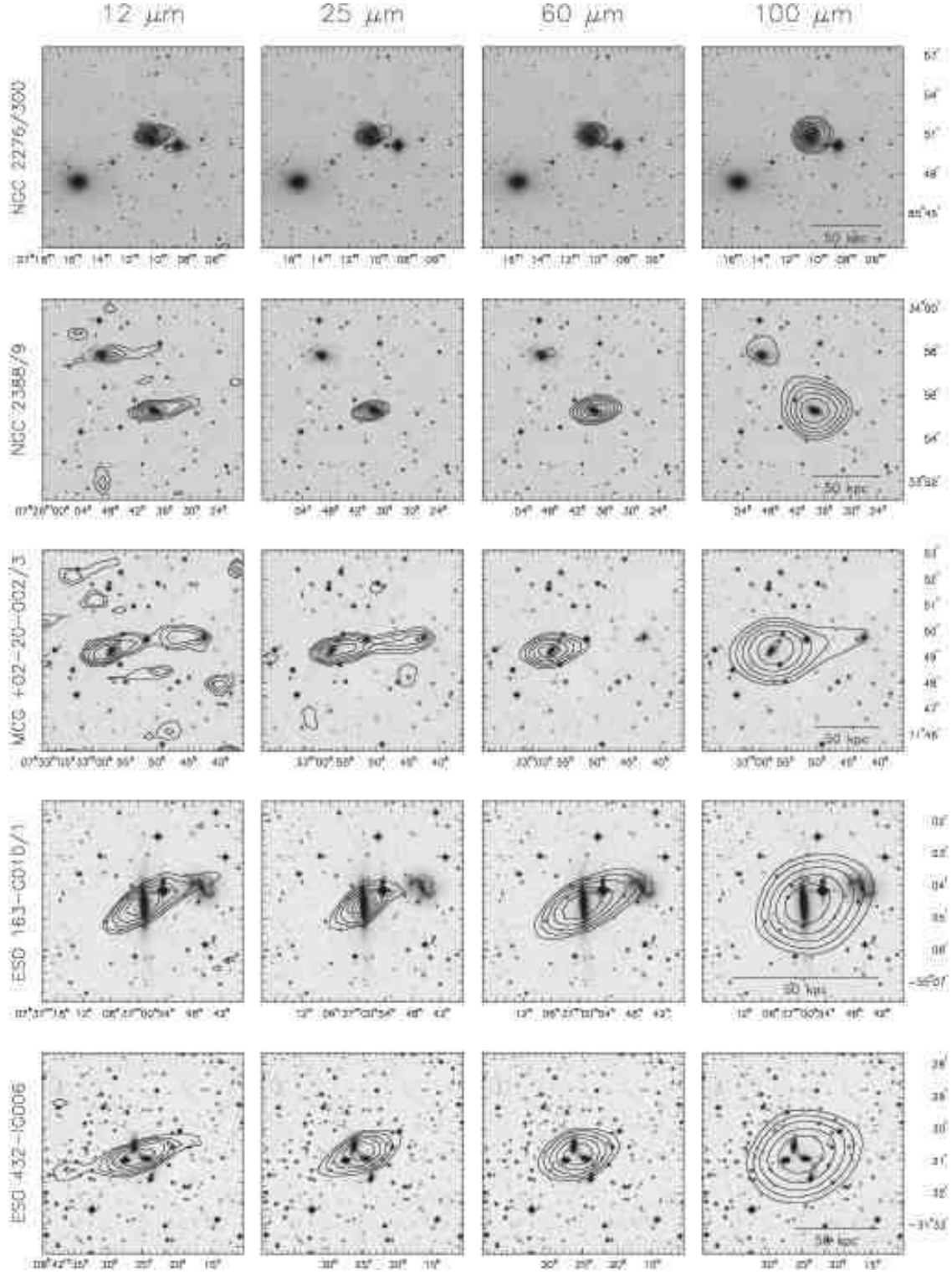


Fig. 1 cont.—

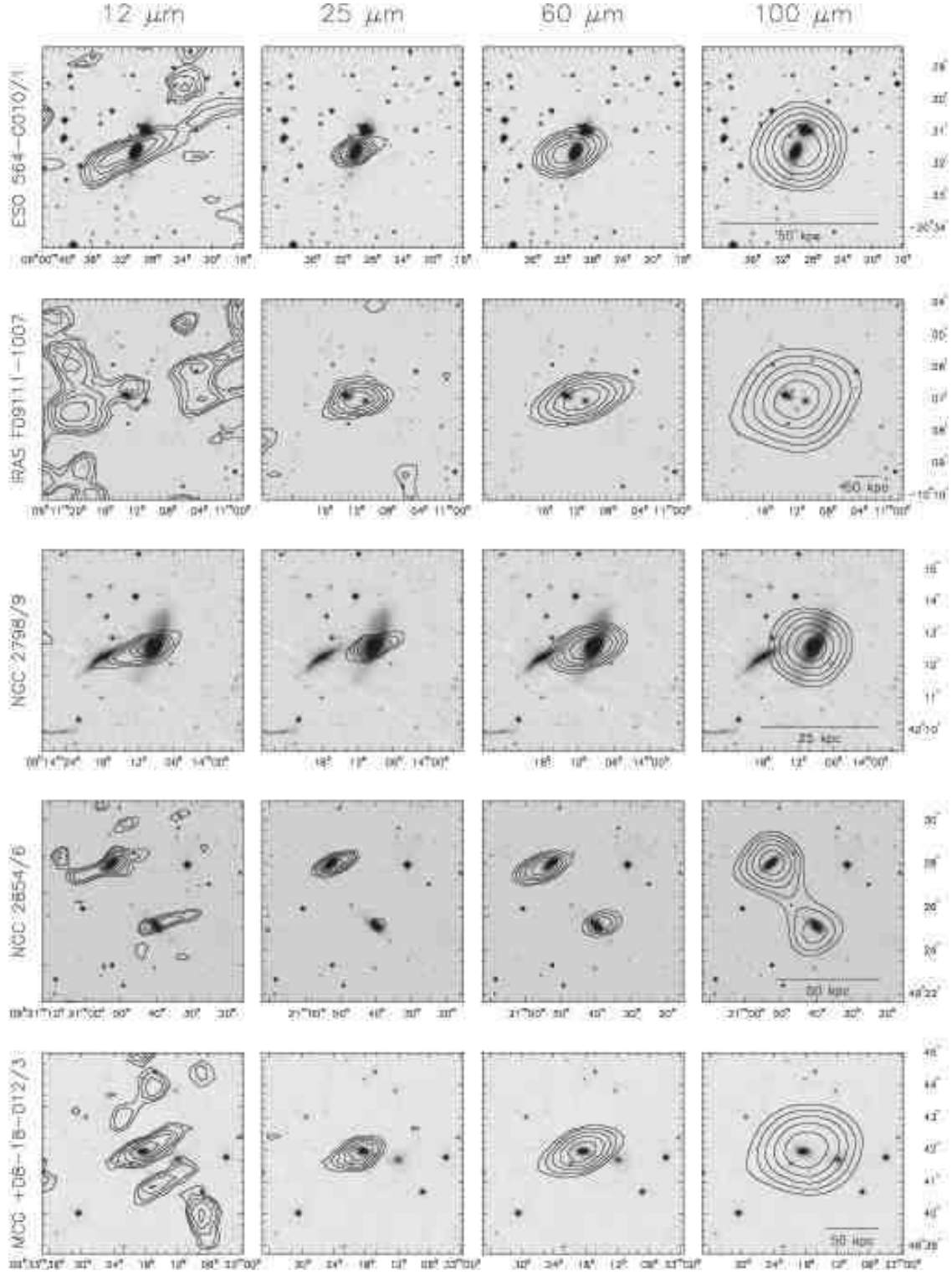


Fig. 1 cont.—

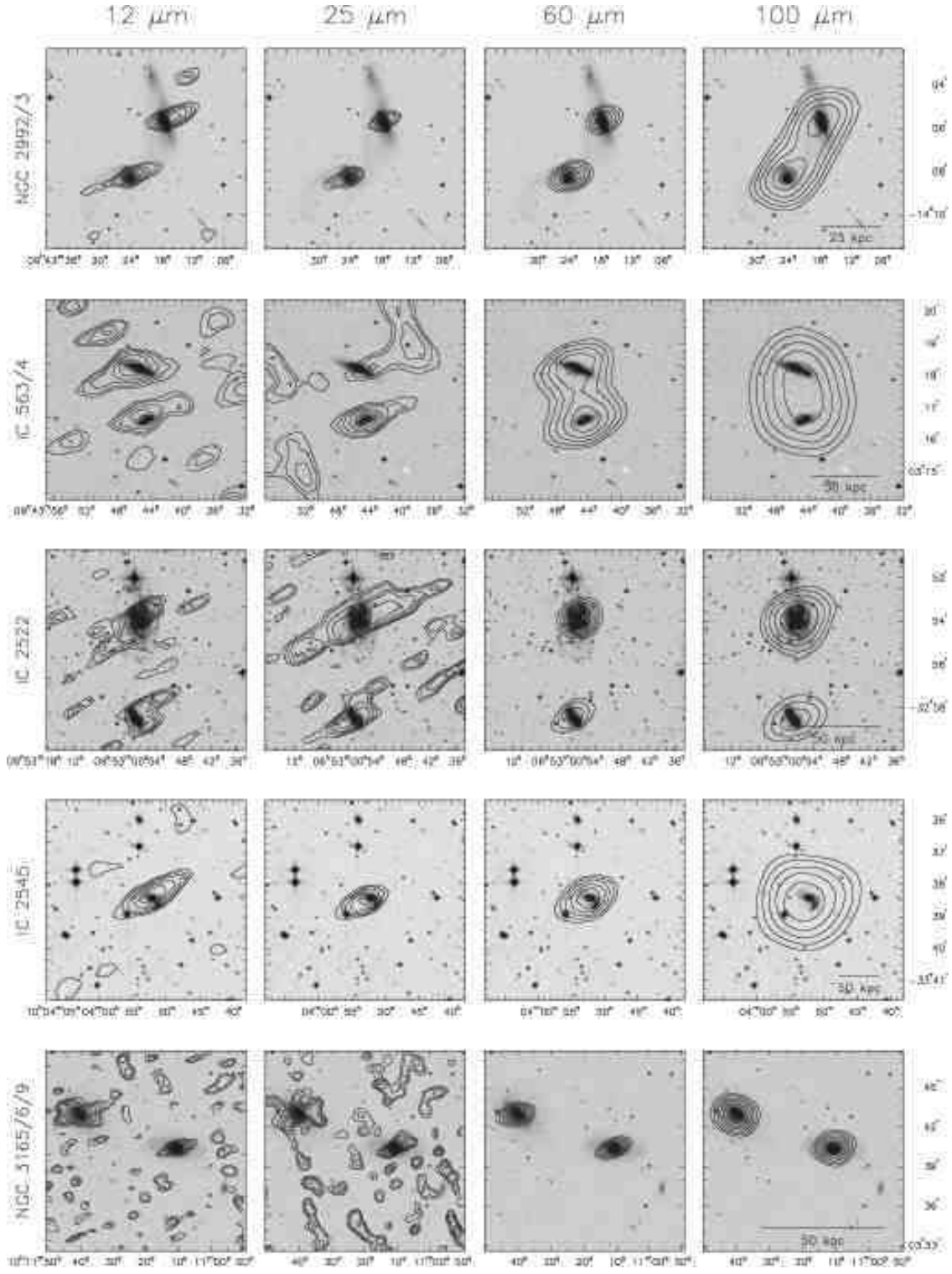


Fig. 1 cont.—

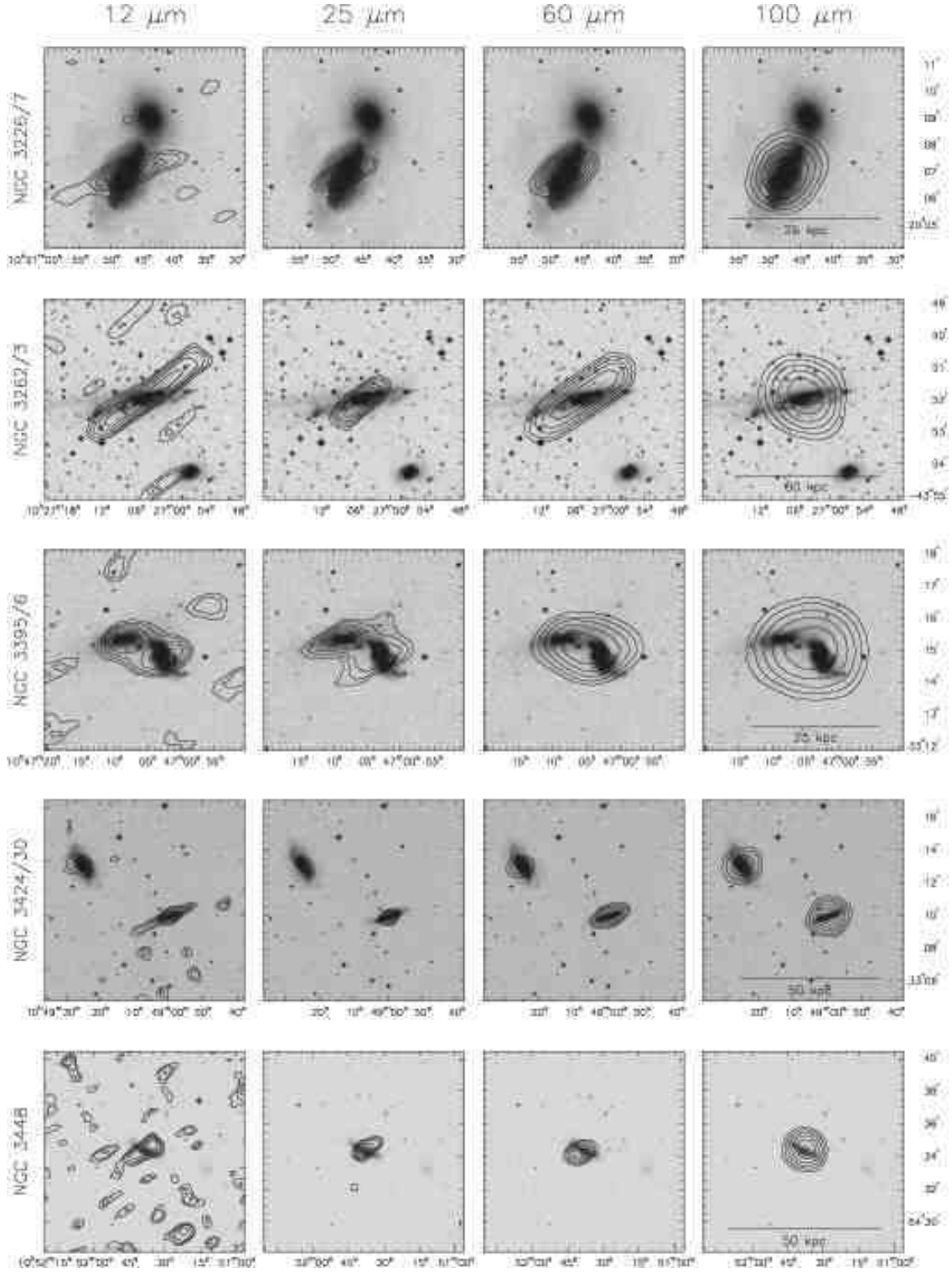


Fig. 1 cont.—



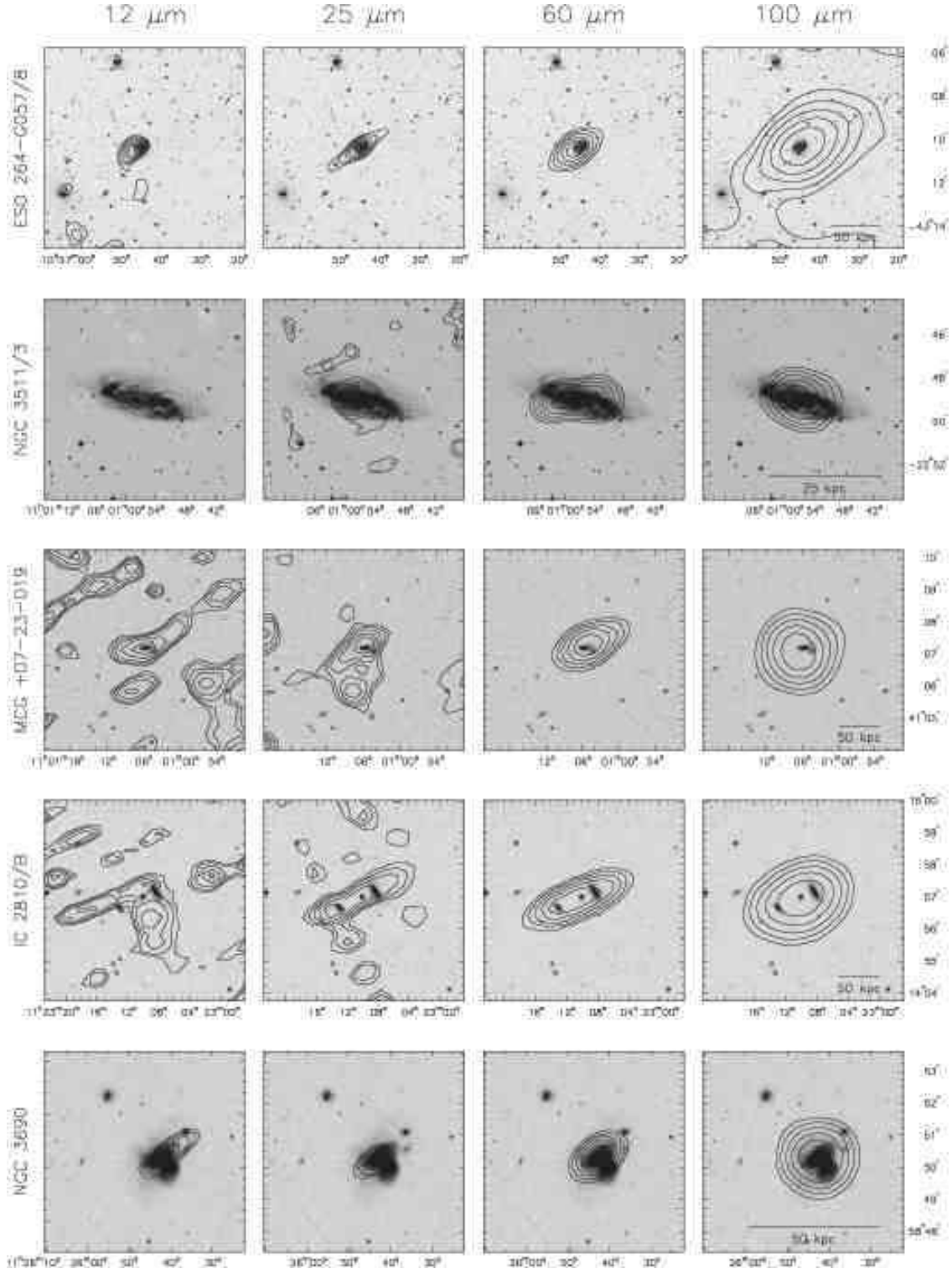


Fig. 1 cont.—



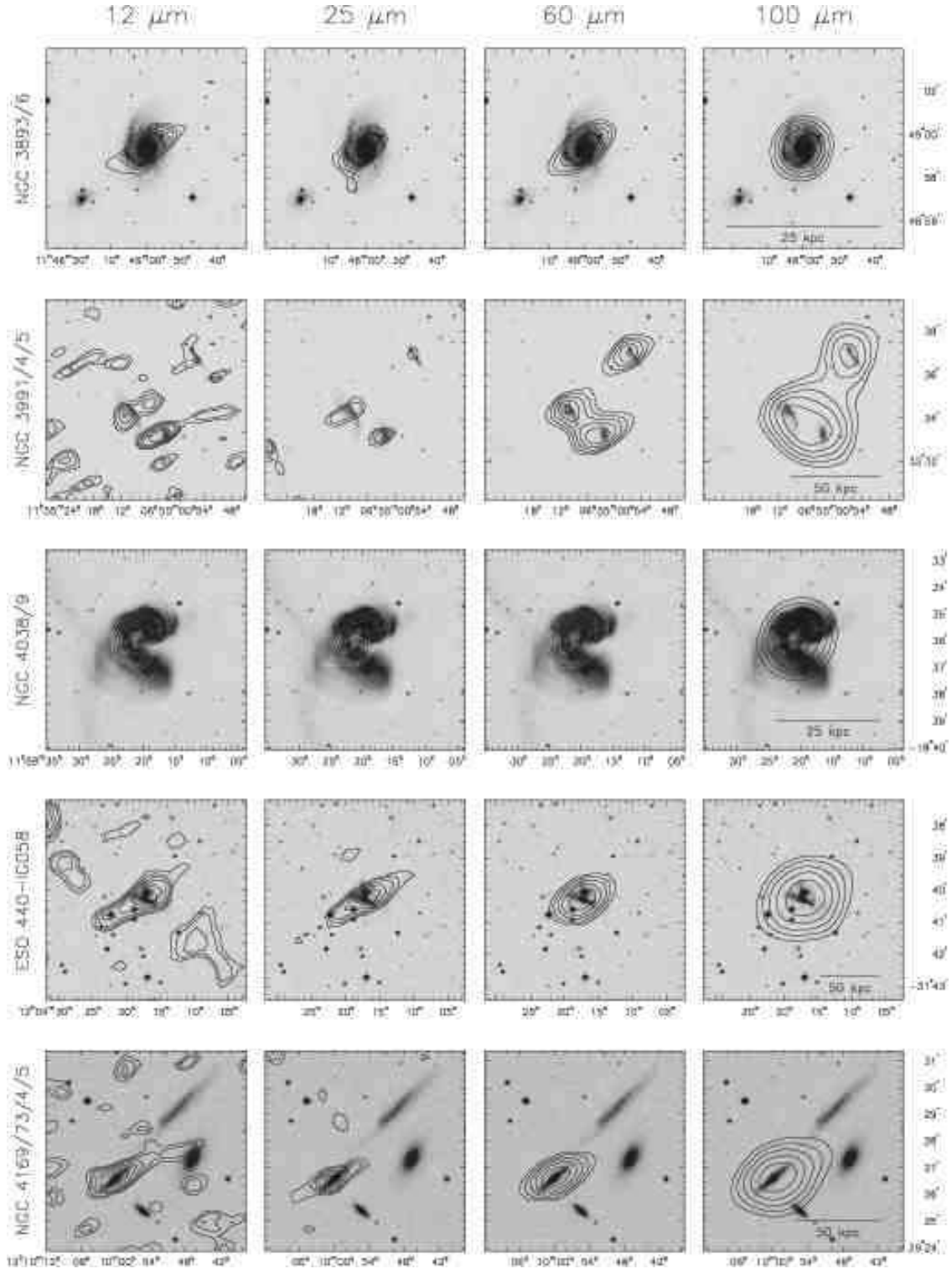


Fig. 1 cont.—

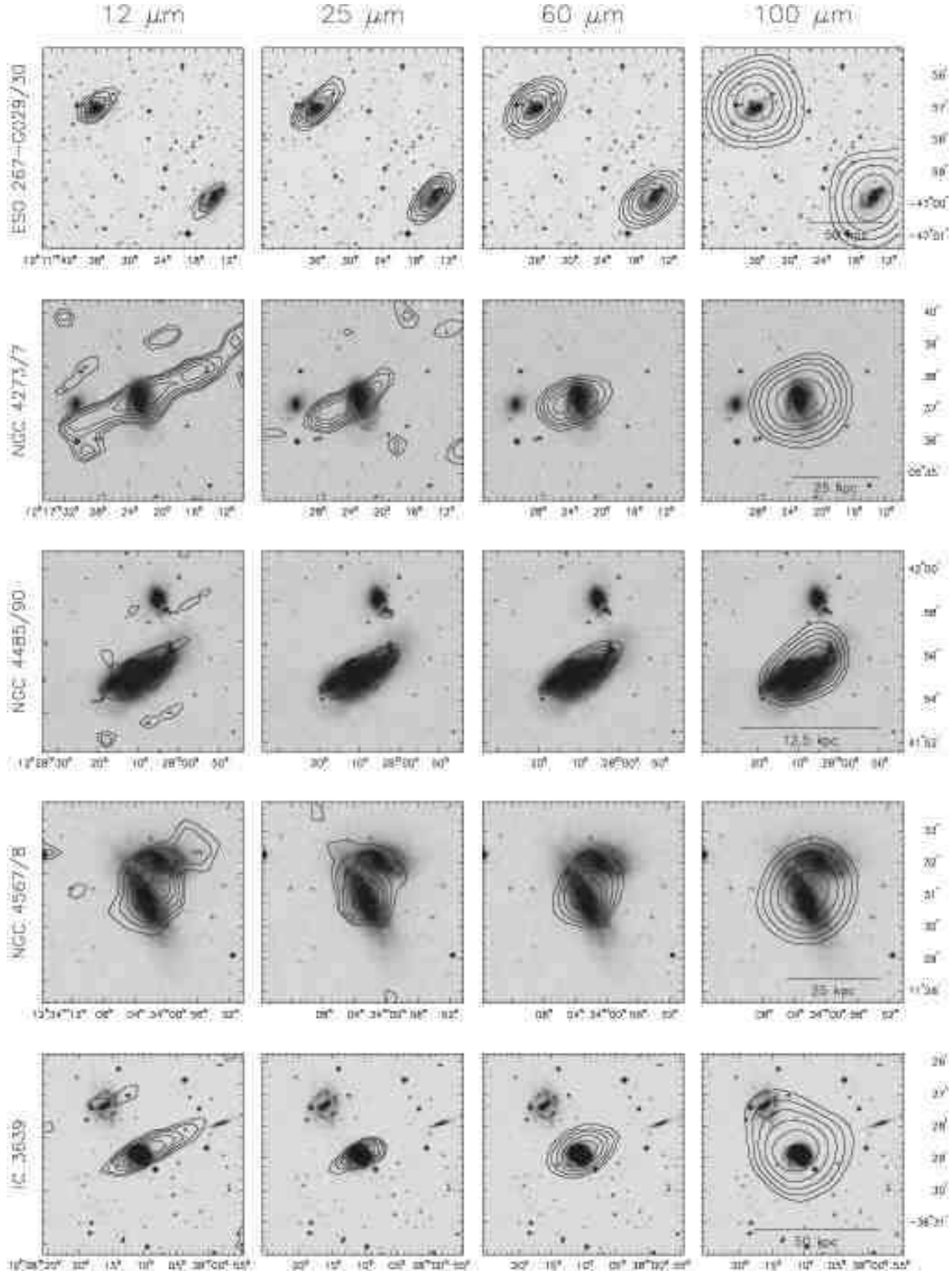


Fig. 1 cont.—

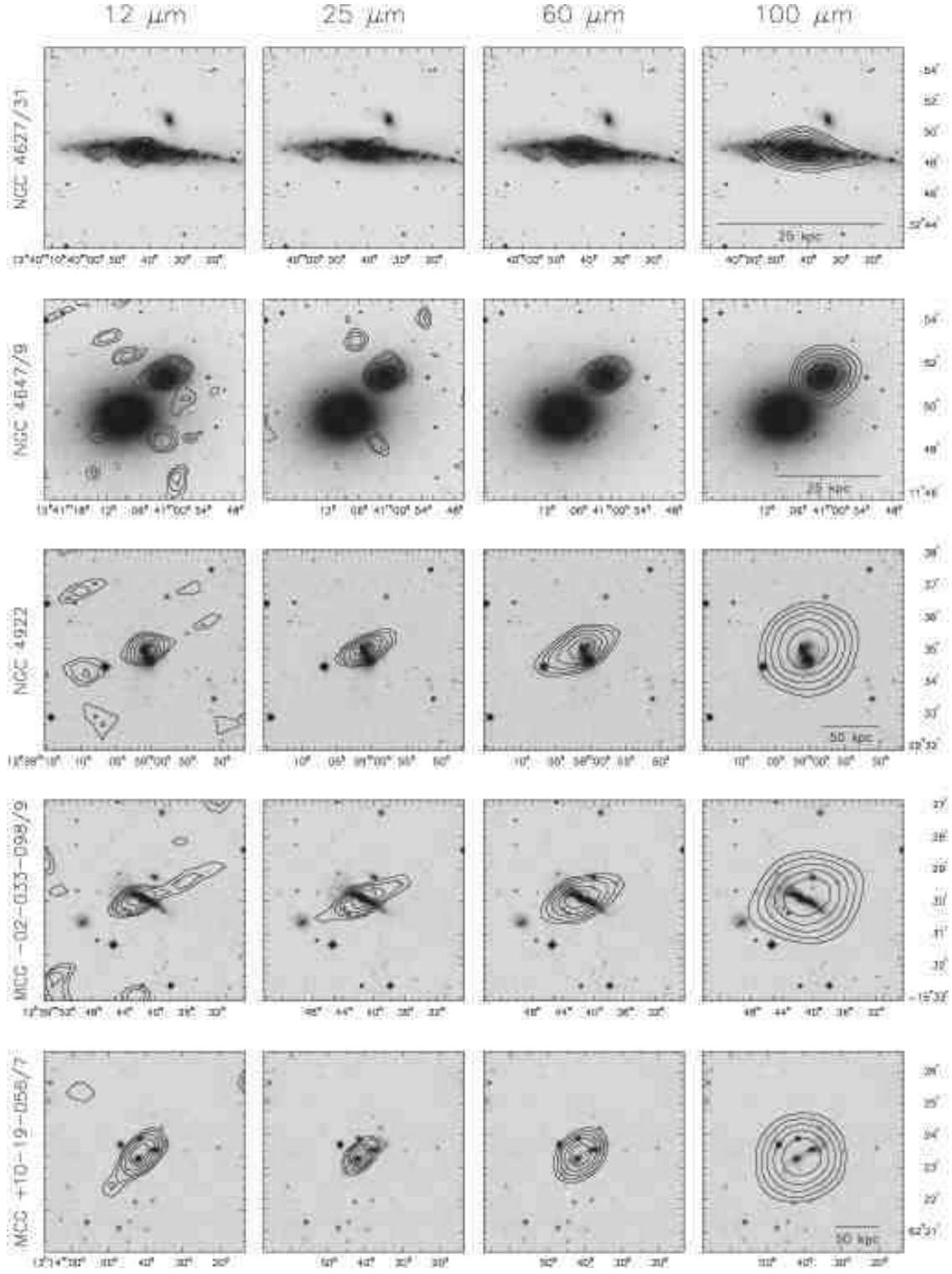


Fig. 1 cont.—

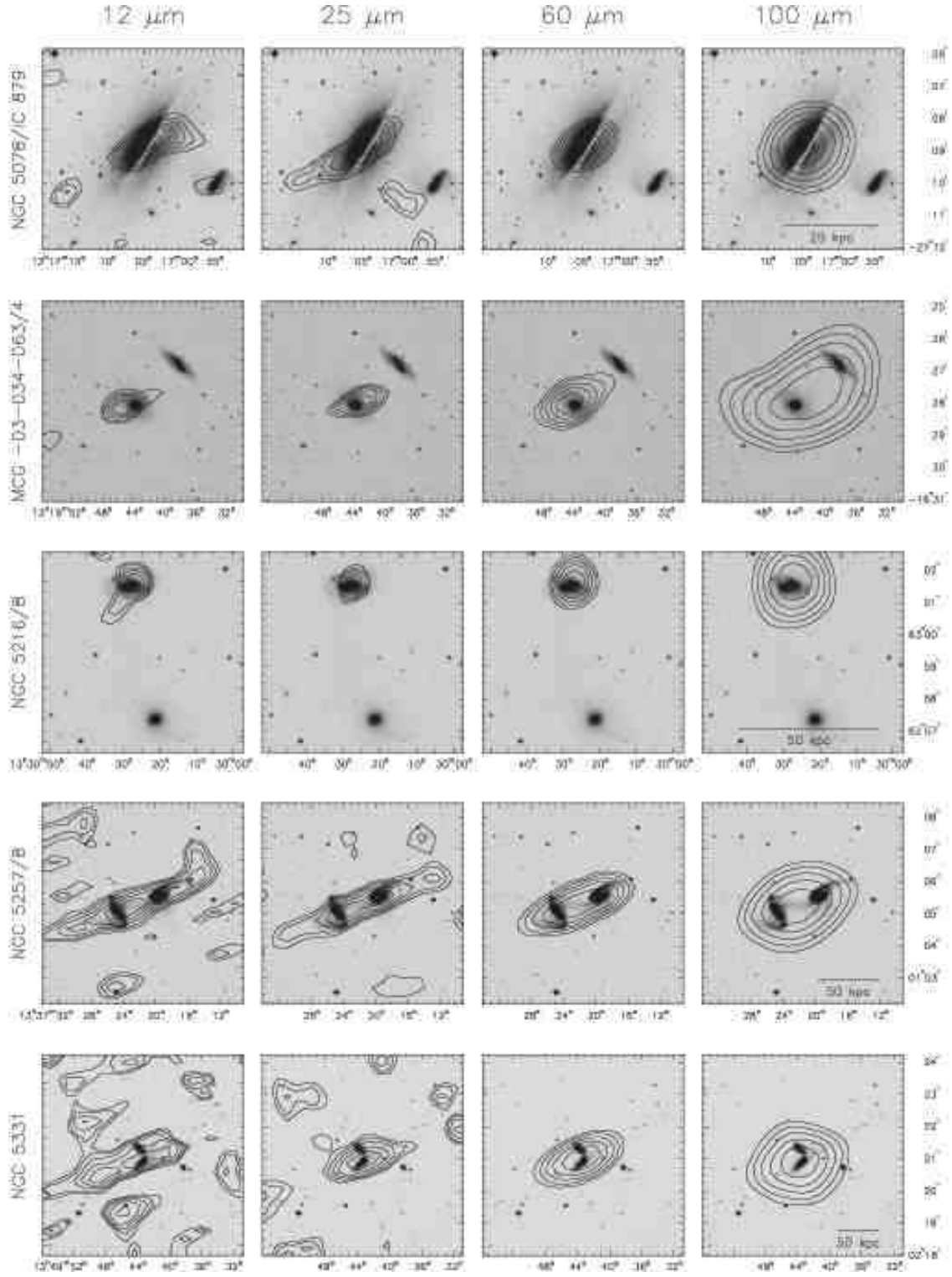


Fig. 1 cont.—

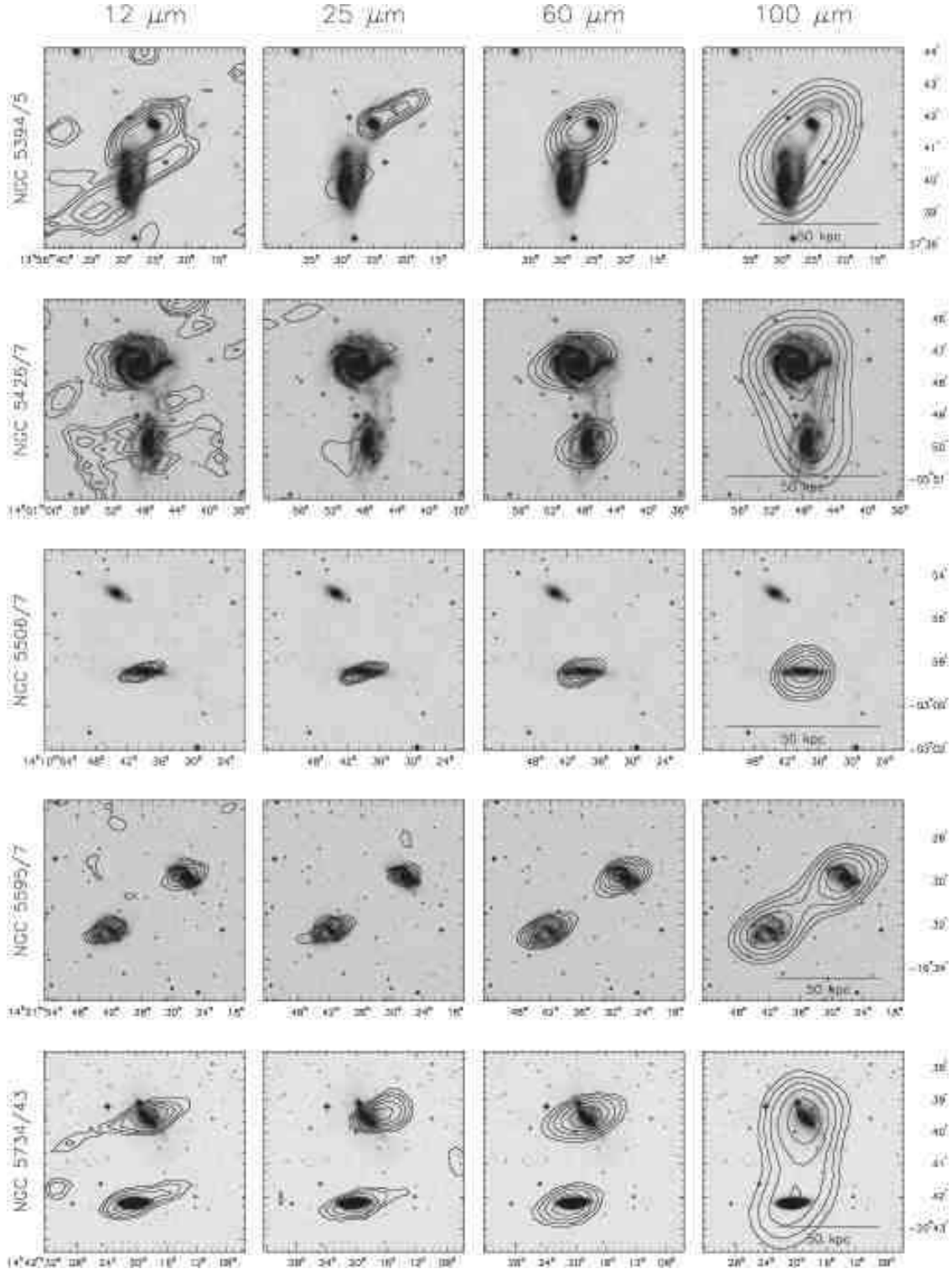


Fig. 1 cont.—

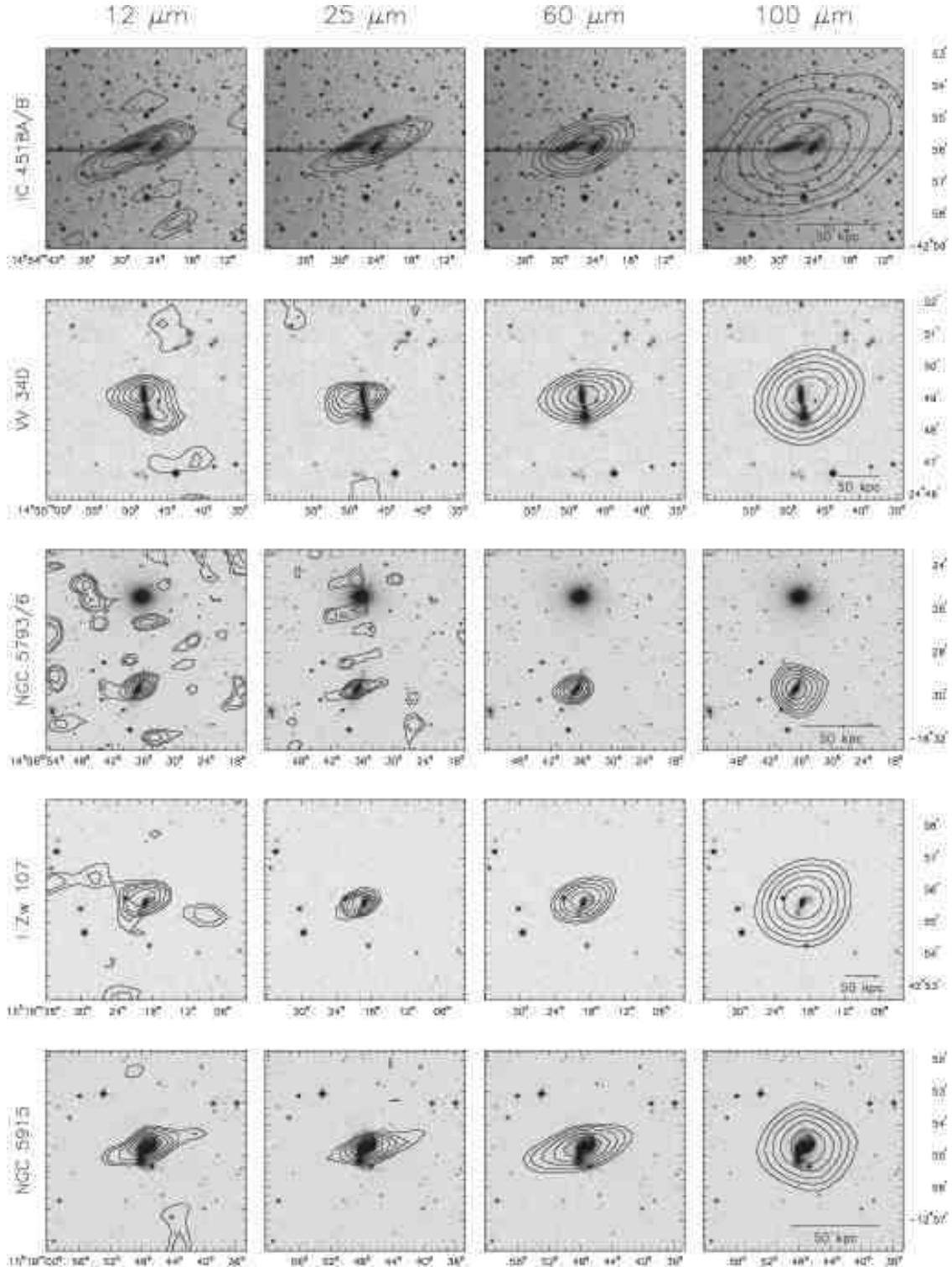


Fig. 1 cont.—

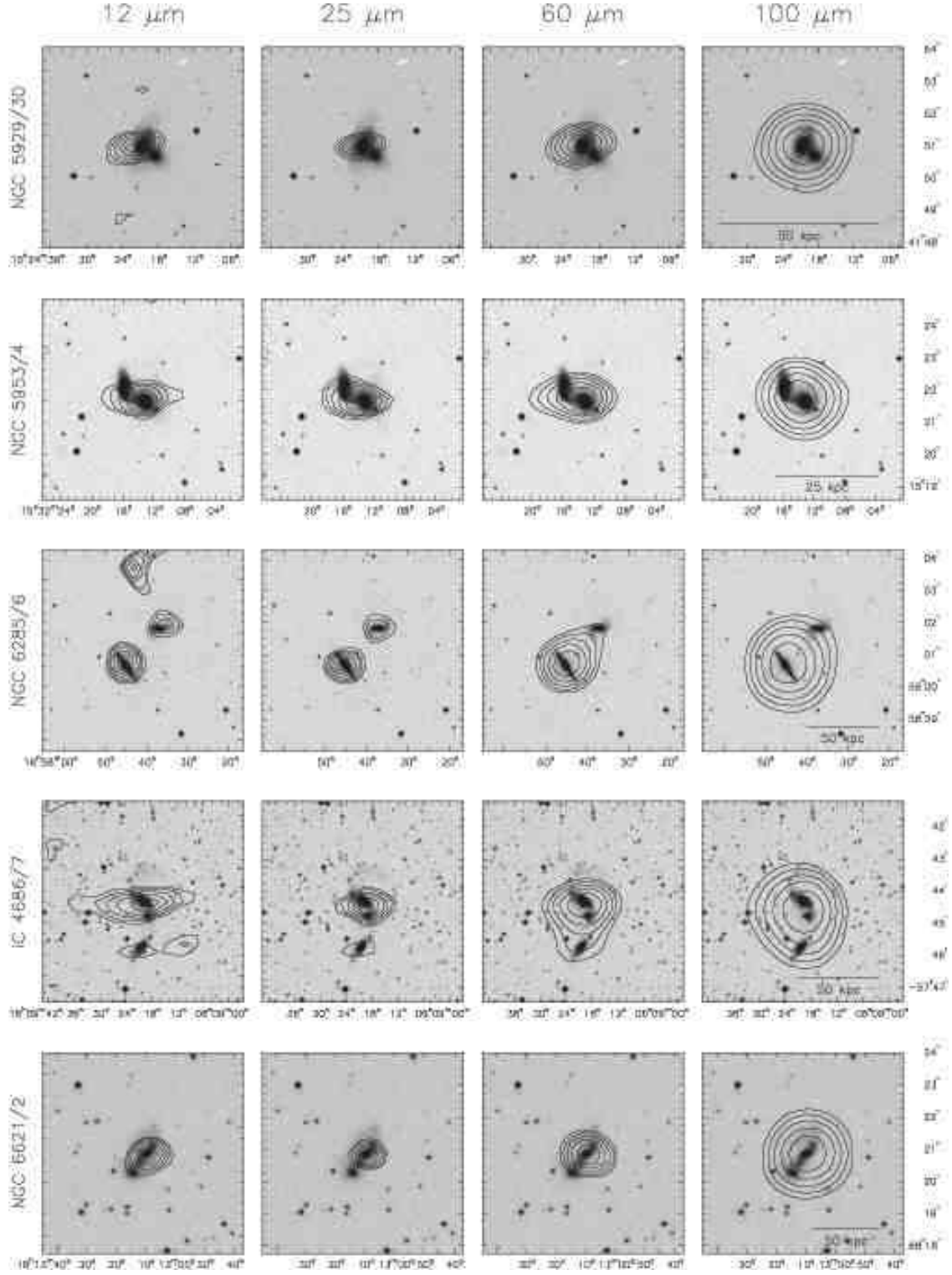


Fig. 1 cont.—



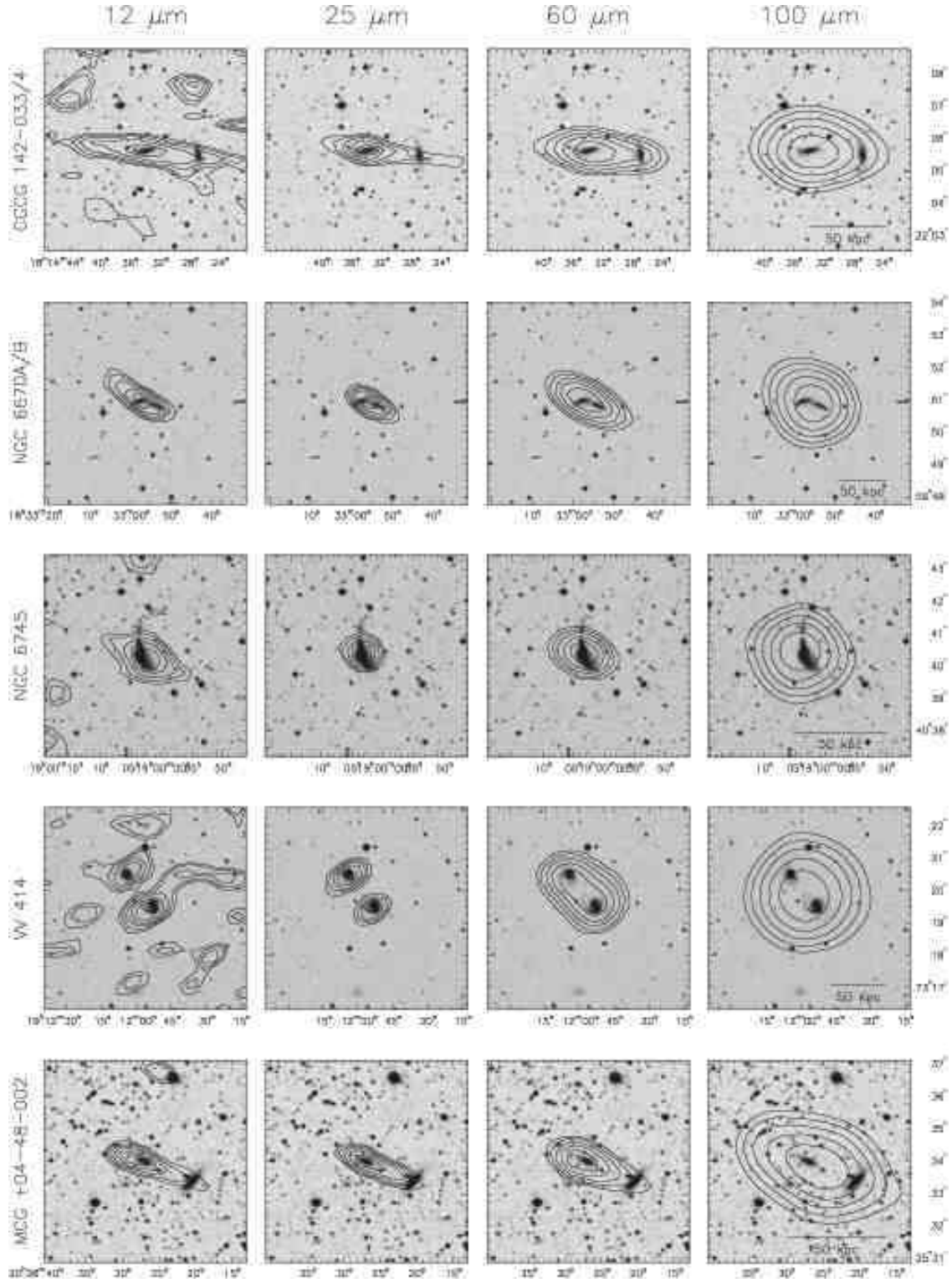


Fig. 1 cont.—



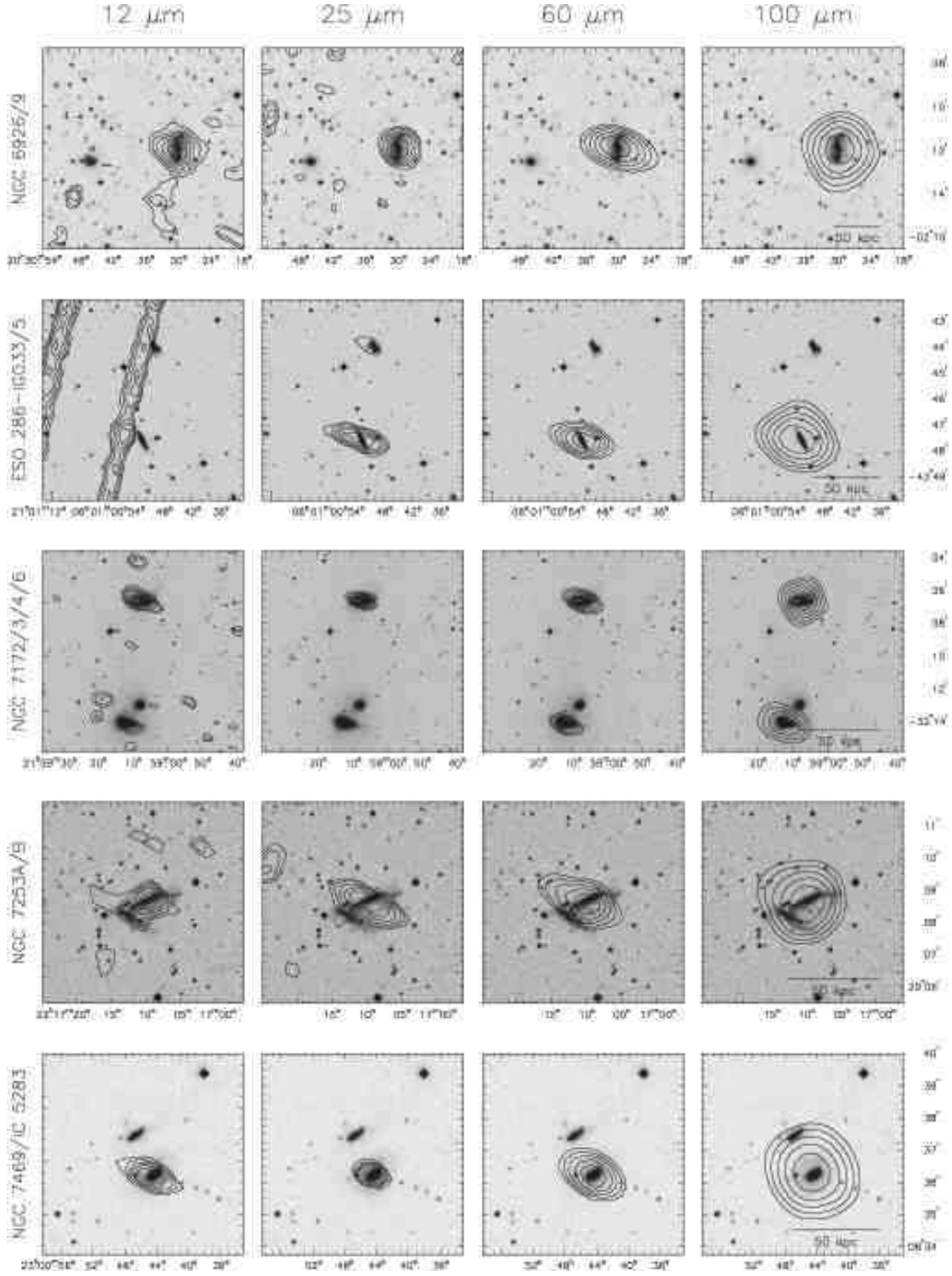


Fig. 1 cont.—

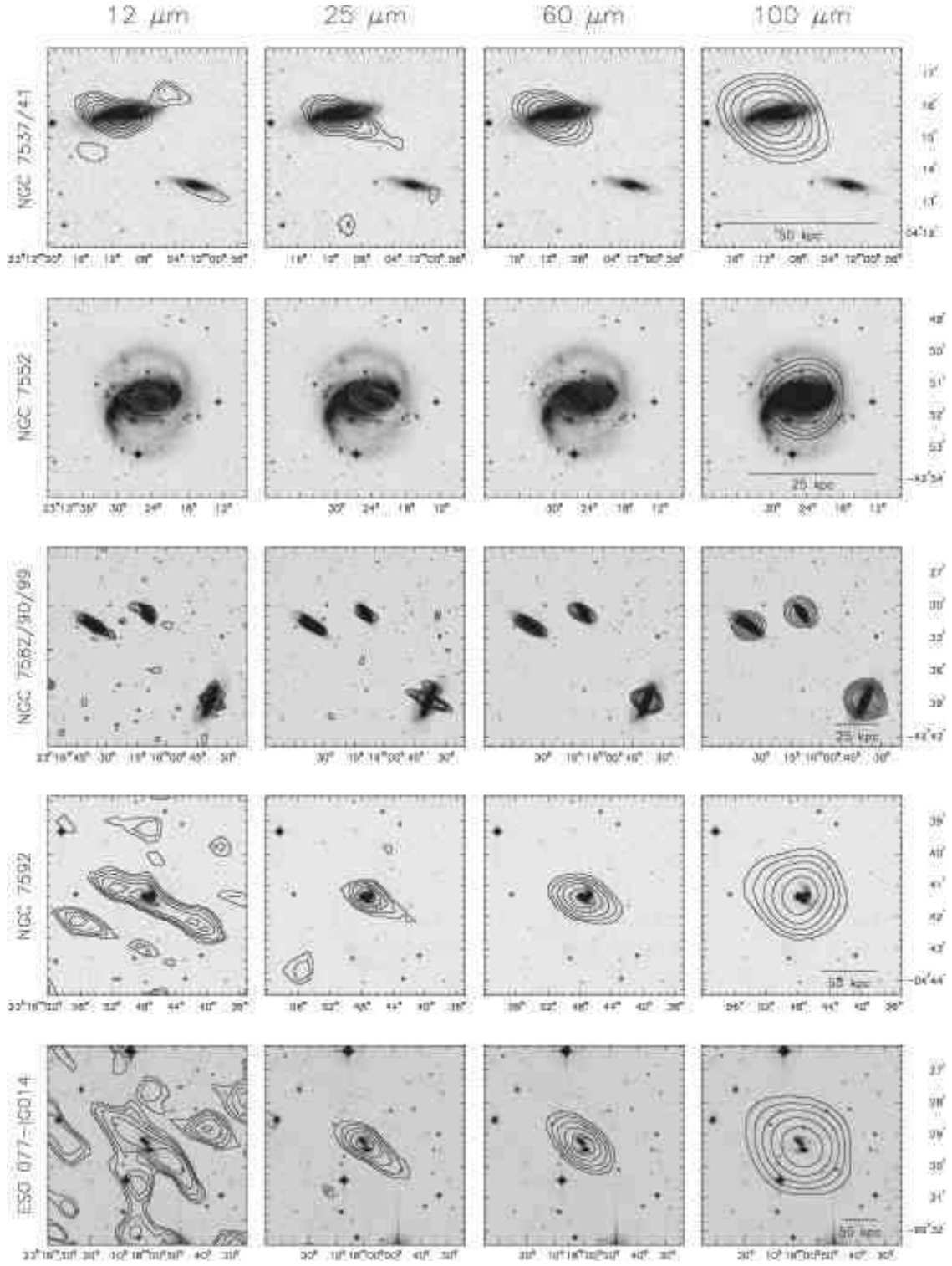


Fig. 1 cont.—

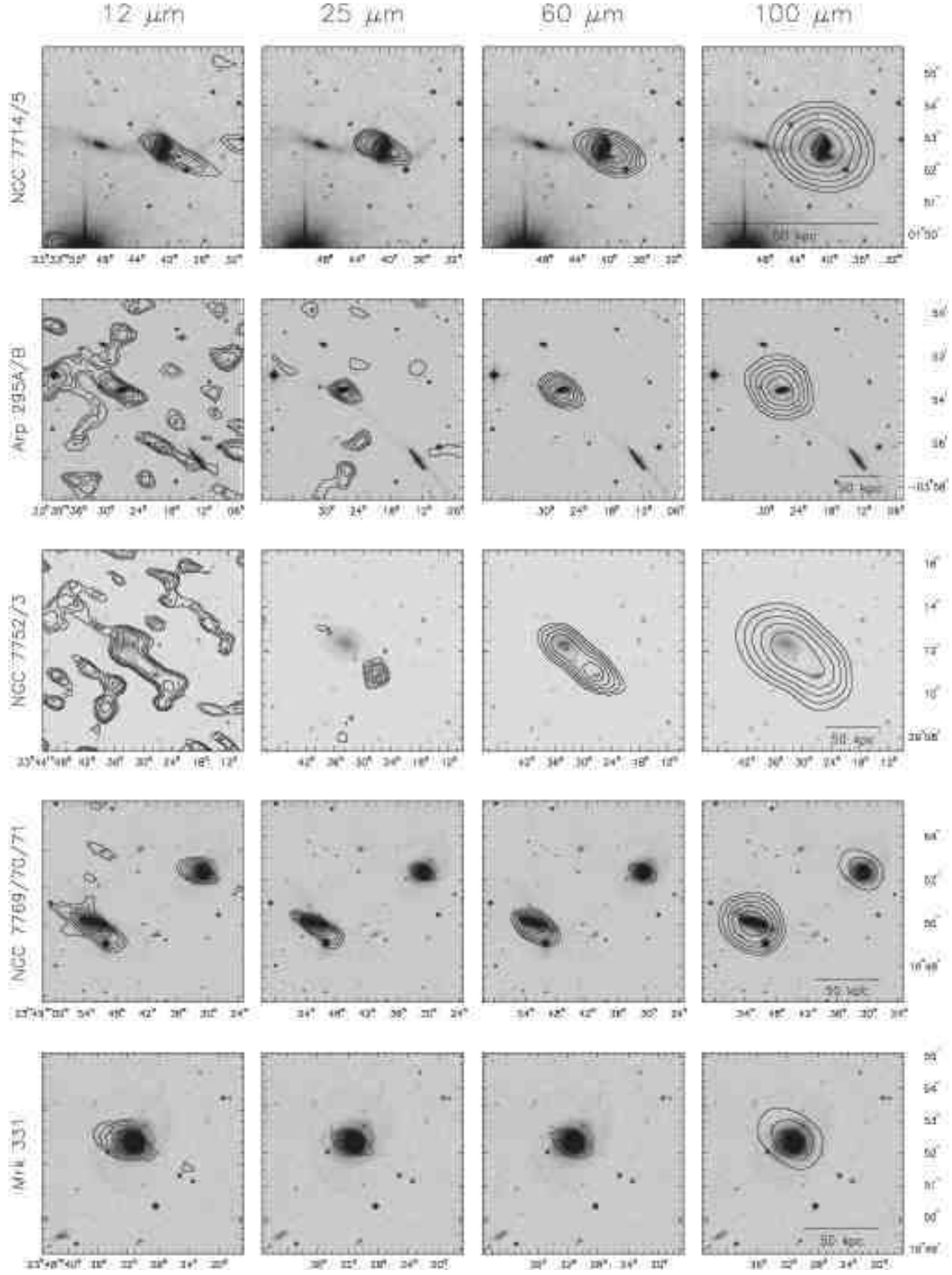


Fig. 1 cont.—

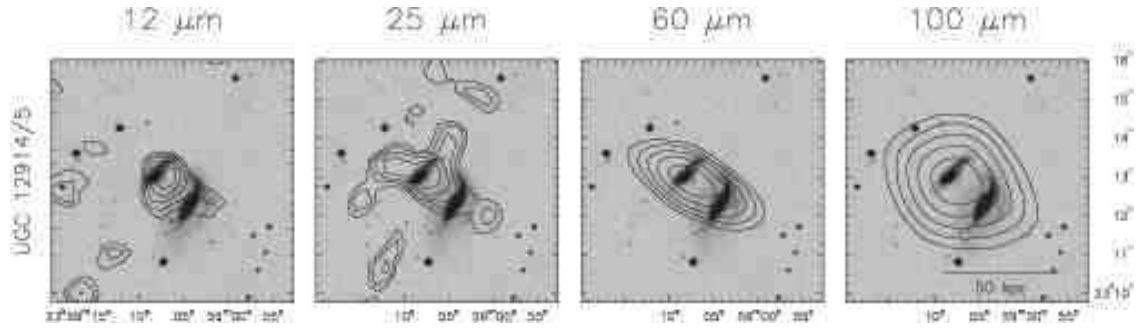


Fig. 1 cont.—

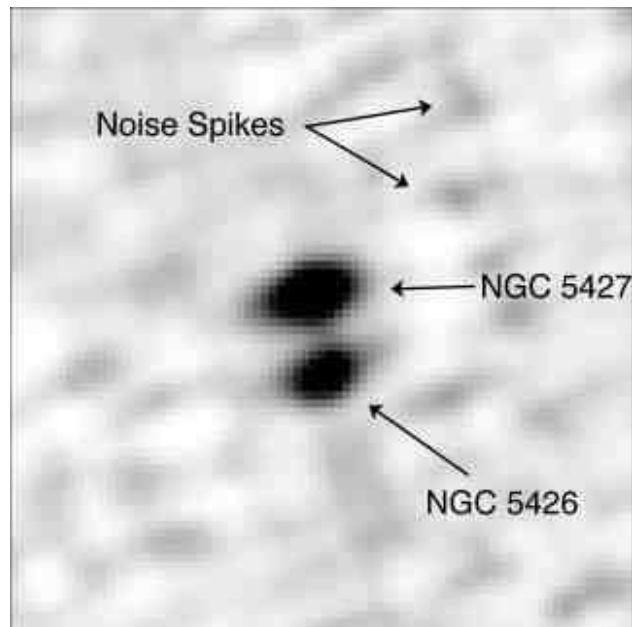


Fig. 2.—

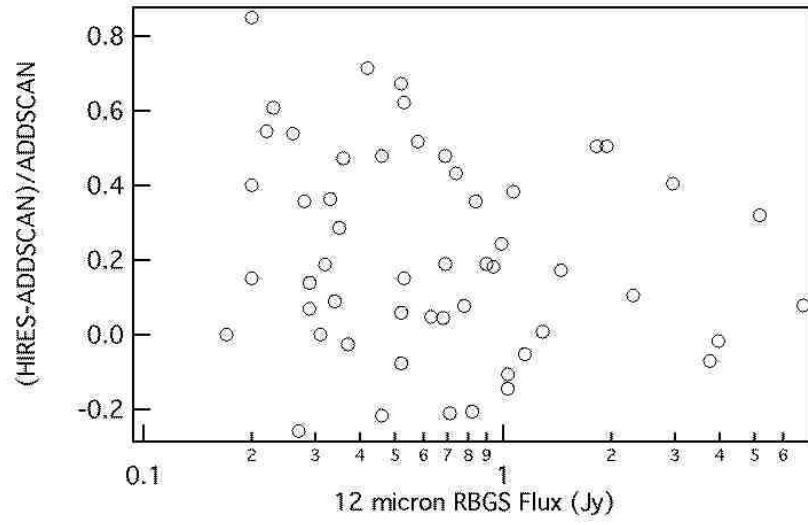


Fig. 3.—

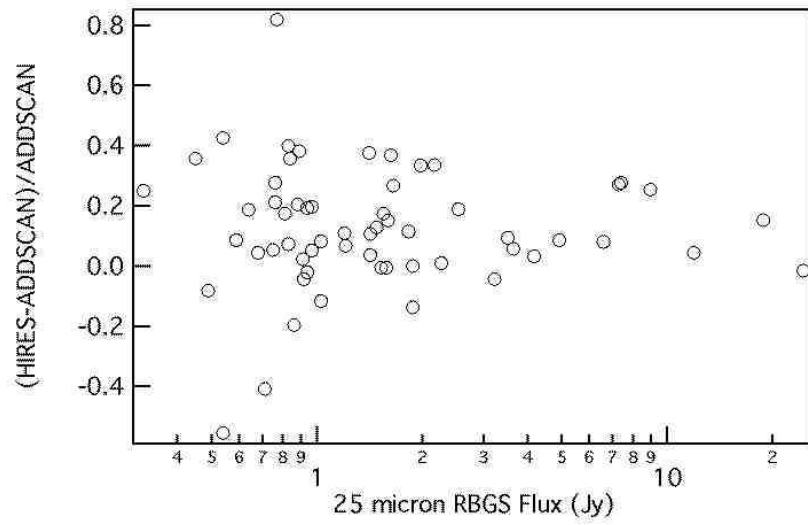


Fig. 4.—

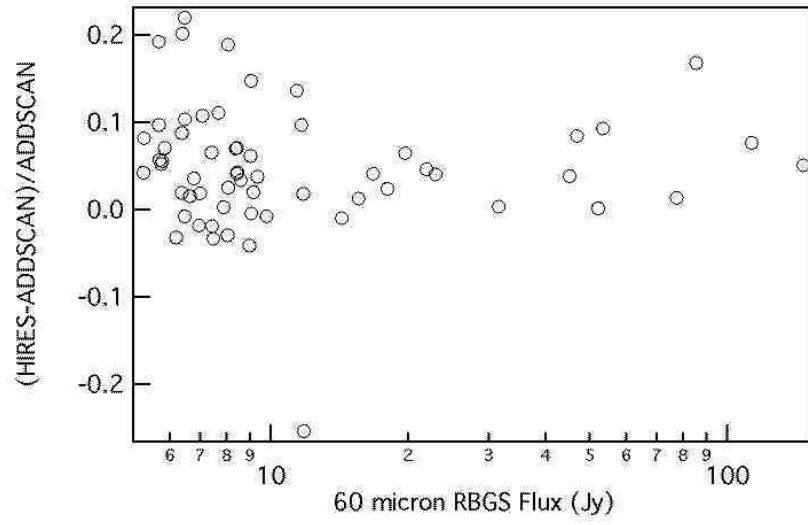


Fig. 5.—

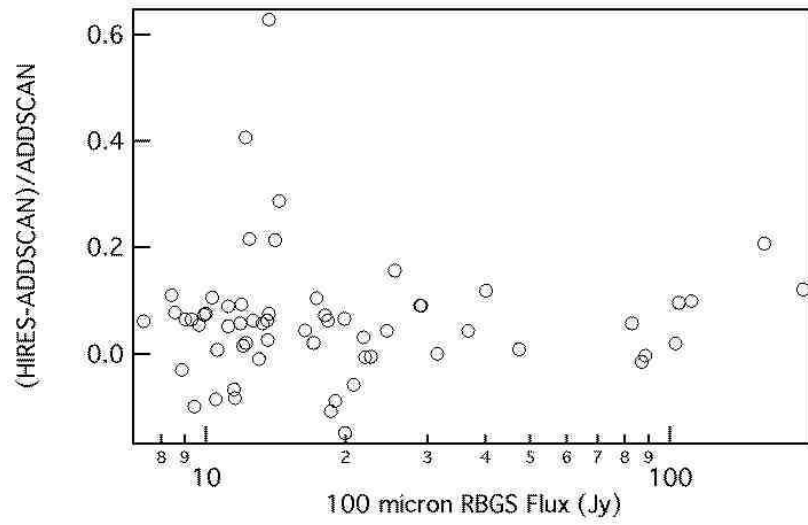


Fig. 6.—

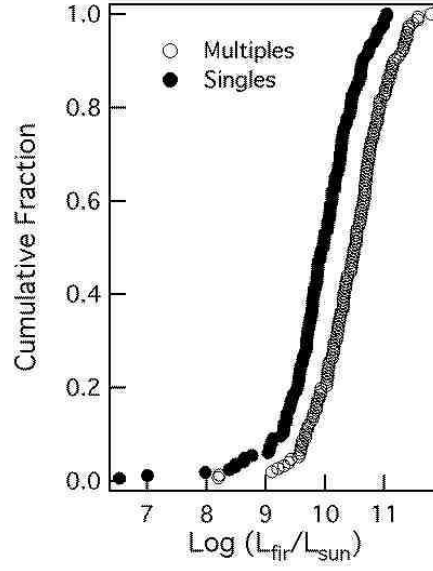


Fig. 7.—

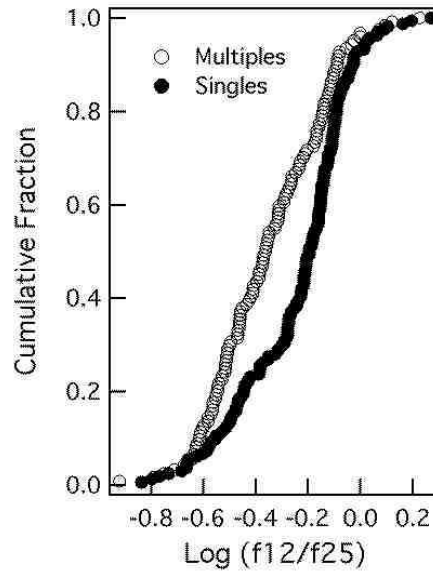


Fig. 8.—



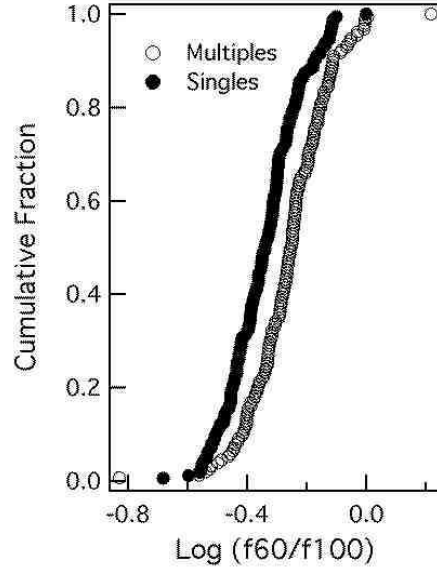


Fig. 9.—

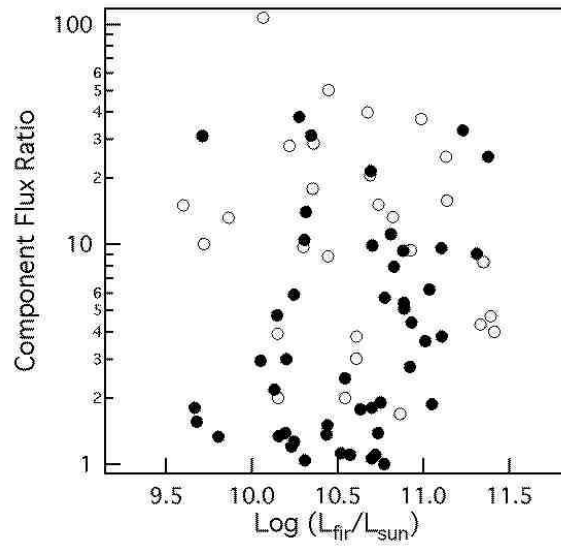


Fig. 10.—

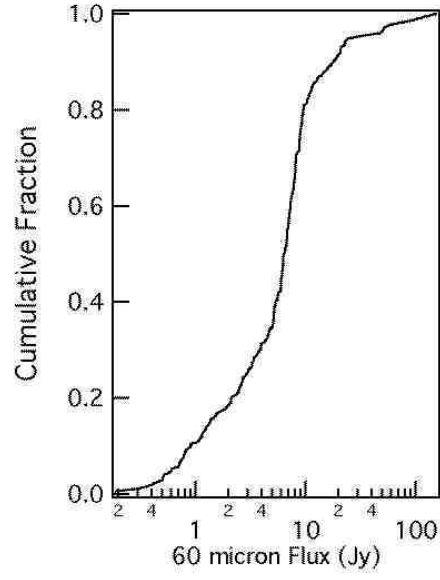


Fig. 11.—

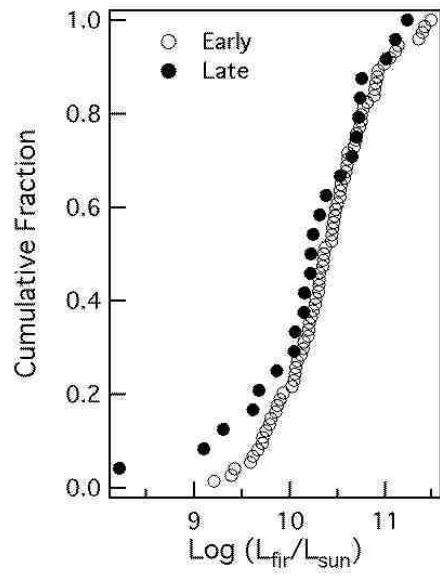


Fig. 12.—

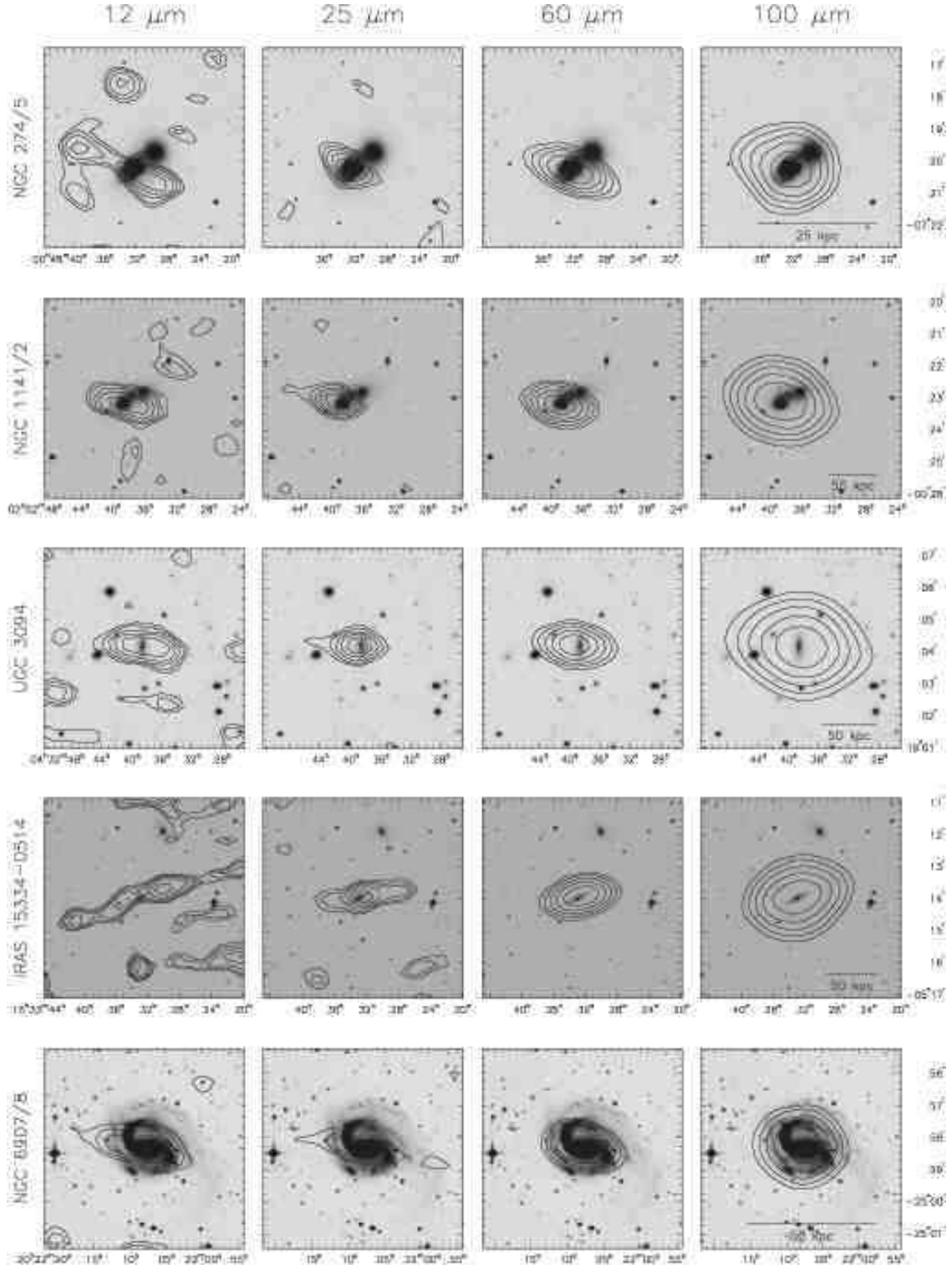


Fig. 13.—

TABLE 1  
INTEGRATED FLUX DENSITIES OF RBGS INTERACTING GALAXIES

Name	RA (B1950) H M S	DEC (B1950) d m s	PT	cz km/s	m <sub>r</sub>	12μm Jy	σ <sub>12</sub> Jy	25μm Jy	σ <sub>25</sub> Jy	60μm Jy	σ <sub>60</sub> Jy	100μm Jy	σ <sub>100</sub> Jy	L <sub>fir</sub> L <sub>⊙</sub>
MCG -02-01-052 = VV 352	00 16 17.2	-10 38 21	I	8193	13.6	< 0.24	...	0.15	0.08	< 0.25	...	< 0.50	...	...
MCG -02-01-051	00 16 18.0	-10 39 16	I	8112	14.8	< 0.24	...	1.19	0.06	7.35	0.12	10.22	1.35	11.13
NGC 230	00 39 59.0	-23 54 12	I	6250	15.4	< 0.30	...	0.38	0.08	1.15	0.09	3.10	0.42	10.22
NGC 232	00 40 17.0	-23 50 06	I	6047	14.5	0.32	0.08	1.22	0.10	9.34	1.80	15.75	4.80	11.01
NGC 235	00 40 24.0	-23 48 54	I	6664	...	< 0.18	...	0.55	0.10	2.67	0.52	3.98	1.24	10.53
MCG +12-02-001	00 50 40.7	72 48 47	I	4706	16.0	0.84	0.10	3.84	0.15	22.93	0.25	31.75	3.00	11.15
NGC 317a = UGC 593	00 54 49.8	43 31 51	O	5293	15.0	< 0.20	...	< 0.25	...	...	...	...	...	...
NGC 317b = UGC 594	00 54 51.1	43 31 23	I	5334	13.8	0.28	0.04	1.15	0.15	9.34	1.00	13.95	1.40	10.88
CGCG 536-014	00 54 52.9	43 25 47	I	5413	15.1	< 0.20	...	< 0.27	...	0.78	0.90	1.97	0.20	9.91
IC 1623 a/b	01 05 21.0	-17 46 23	I	6016	14.3	0.92	0.10	3.86	0.20	23.85	0.20	31.53	0.25	11.37
IC 1622	01 05 09.0	-17 48 18	O	6343	15.1	< 0.30	...	< 0.20	...	0.50	0.20	1.25	0.25	9.86
NGC 520 <sup>2</sup>	01 21 59.6	03 31 51	I	2281	12.0	1.07	0.20	3.08	0.45	31.62	2.00	47.76	3.30	10.68
NGC 633	01 34 10.6	-37 34 33	I	5148	13.5	0.22	0.03	0.72	0.08	2.01 <sup>4</sup>	0.54	2.32 <sup>4</sup>	1.00	10.15
ESO 297-G012	01 34 12.3	-37 35 41	I	5193	14.9	0.34	0.02	0.96	0.07	6.24 <sup>4</sup>	1.40	11.01 <sup>4</sup>	4.20	10.71
UGC 1385 = Mrk 2	01 51 56.3	36 40 18	I	5621	13.9	0.39	0.06	1.15	0.14	5.92	0.70	9.27	1.10	10.74
CGCG 522-061	01 51 59.1	36 37 08	I	4919	15.2	< 0.28	...	< 0.20	...	0.51	0.07	< 0.76	...	...
CGCG 522-062	01 52 04.3	36 40 31	O	5621	15.2	< 0.20	...	< 0.25	...	< 0.25	...	< 0.85	...	...
NGC 833 = Arp 318	02 06 53.3	-10 22 09	O	3864	13.7	< 0.30	...	< 0.30	...	< 0.12	...	< 0.40	...	...
NGC 835 = Mrk 1021	02 06 57.3	-10 22 19	I	4152	12.9	0.45	0.15	0.97	0.30	6.33	0.65	11.54	1.20	10.53
NGC 838	02 07 11.1	-10 22 57	I	3851	13.6	0.92	0.15	2.70	0.30	12.96	1.40	16.96	1.50	10.72
NGC 839	02 07 15.6	-10 25 11	I	3847	13.9	0.68	0.15	3.34	0.30	12.80	1.40	12.90	1.40	10.68
UGC 1720b	02 11 18.9	04 56 06	O	9200	15.5	< 0.18	...	< 0.30	...	< 0.30	...	< 0.60	...	...
UGC 1720 = IC 214	02 11 29.2	04 56 28	I	9061	15.4	0.33	0.10	0.68	0.23	5.58	0.25	9.23	0.30	11.14
NGC 876	02 15 10.0	14 17 26	I	3860	16.5	...	...	...	...	4.62	1.30	...	...	...
NGC 877	02 15 15.3	14 19 01	I	3913	12.6	1.14	0.12	1.94	0.41	8.82	1.50	29.55	2.00	10.75
MCG +05-06-035 = Mrk 1034 Ned01	02 20 20.8	31 57 42	O	10083	15.4	< 0.21	...	< 0.20	...	< 1.60	...	...	...	...
MCG +05-06-036 = Mrk 1034 Ned02	02 20 23.6	31 57 56	I	10121	15.0	0.30	0.08	0.69	0.11	6.83	1.10	12.15	1.20	11.33
NGC 1097	02 44 10.6	-30 29 02	I	1275	10.2	4.16	0.42	9.27	0.95	58.29	6.00	114.82	14.00	10.48
UGC 2369 Ned 02	02 51 15.7	14 46 25	O	9947	15.5	...	...	< 0.40	...	< 1.00	...	...	...	...
UGC 2369 Ned 01	02 51 15.9	14 46 03	I	9804	15.5	0.37	0.11	1.62	0.21	8.27	0.20	11.75	0.40	11.35
NGC 1270	03 15 39.6	41 17 19	O	4871	14.3	< 0.20	...	< 0.50	...	0.38	0.05	< 0.80	...	...
NGC 1272	03 16 02.8	41 18 35	O	4021	12.9	< 0.20	...	< 0.40	...	< 0.40	...	< 0.40	...	...
NGC 1273	03 16 08.2	41 21 34	O	5351	14.3	< 0.20	...	< 0.40	...	< 0.80	...	< 0.50	...	...
UGC 2665	03 16 08.6	41 27 15	I	7806	15	< 0.20	...	< 0.40	...	0.72	0.10	1.23	0.15	10.12
IC 1907	03 16 15.6	41 23 58	O	4420	15.4	< 0.20	...	< 0.40	...	< 0.40	...	< 0.50	...	...
NGC 1274	03 16 21.9	41 22 05	O	6447	15.1	< 0.20	...	< 0.40	...	< 0.30	...	< 0.30	...	...
NGC 1275	03 16 28.7	41 19 48	I	5260	12.6	0.93	0.10	3.02	0.31	7.09	0.75	7.60	0.90	10.70
NGC 1277/8	03 16 34.8	41 23 12	I	4982	...	< 0.20	...	< 0.40	...	0.52	0.05	< 0.70	...	...
NGC 1281	03 16 47.2	41 26 58	O	4201	14.5	< 0.20	...	< 0.40	...	< 0.90	...	< 0.90	...	...
NGC 1283	03 16 57.0	41 13 06	O	6749	14.7	< 0.20	...	< 0.40	...	0.43	0.05	< 0.40	...	...
IRAS 03217+4022	03 21 47.6	40 23 01	I	7007	...	< 0.28	...	1.12	0.17	7.92	0.37	13.19	0.41	11.07
CGCG 468-002	05 05 26.9	17 18 23	I	5454	13.5	< 0.30	...	0.15	0.10	7.21	1.00	11.15	2.00	10.79
UGC 3405	06 04 45.3	80 29 15	I	3791	15.3	0.14	0.05	0.20	0.04	1.93 <sup>4</sup>	0.31	6.08 <sup>4</sup>	1.80	10.05
UGC 3410	06 05 19.2	80 27 44	I	3887	15.0	0.49	0.05	0.90	0.07	7.69 <sup>4</sup>	1.15	18.32 <sup>4</sup>	5.10	10.61
NGC 2146	06 10 40.1	78 22 23	I	893	11.4	7.36	0.80	21.66	2.40	154.12	16.00	217.44	24.00	10.54

TABLE 1—*Continued*

Name	RA (B1950) H M S	DEC (B1950) d m "	PT	cz km/s	m <sub>z</sub>	12μm Jy	σ <sub>12</sub> Jy	25μm Jy	σ <sub>25</sub> Jy	60μm Jy	σ <sub>60</sub> Jy	100μm Jy	σ <sub>100</sub> Jy	L <sub>fir</sub> L <sub>⊙</sub>
NGC 2207	06 14 14.4	-21 21 15	O	2741	12.2	1.02	0.20	2.00	0.20	19.9	0.18	43.40	0.16	10.70
IC 2163	06 14 20.3	-21 21 26	O	2765	11.6	0.58	0.20	1.10	0.20	...	...	...	...	...
NGC 2221	06 19 27.5	-57 33 15	I	2532	13.8	0.34	0.05	0.62	0.20	5.35	0.50	11.10	0.50	10.05
NGC 2222	06 19 28.0	-57 30 34	I	2602	14.2	0.18	0.05	0.18	0.05	2.11	0.50	3.30	0.50	9.62
ESO 161-G001	06 19 45.1	-57 28 27	I	...	14.8	< 0.15	...	< 0.15	...	0.71	0.20	0.72	0.20	...
ESO 255-IG007 Ned 01/02/03	06 26 01.0	-47 08 48	I	11637	...	0.38	0.08	1.57	0.23	10.38	0.10	12.52	0.30	11.57
ESO 557-G001	06 29 32.3	-17 36 41	I	...	15.7	< 0.50	...	< 0.30	...	1.23	0.20	...	...	...
ESO 557-G002	06 29 33.9	-17 35 06	I	6385	15.0	< 0.50	...	0.69	0.09	6.67	0.20	9.60	1.00	10.89
NGC 2341	07 06 14.4	20 41 05	I	5227	13.8	0.66	0.06	1.13	0.12	7.62	1.22	9.88 <sup>4</sup>	2.97	10.75
NGC 2342	07 06 17.4	20 43 10	I	5276	13.1	1.00	0.10	1.76	0.19	7.99	1.30	16.66 <sup>4</sup>	4.40	10.86
ESO 491-G020	07 07 47.0	-27 29 18	I	2955	13.8	0.70	0.30	2.30	0.50	16.42	2.00	23.80	2.90	10.61
ESO 491-G021	07 07 49.0	-27 29 36	O	2847	13.6	< 0.30	...	< 0.60	...	...	...	...	...	...
NGC 2276	07 10 18.4	85 51 00	I	2417	11.9	1.48	0.20	2.23	0.20	14.15	1.23	31.58	1.73	10.45
NGC 2300	07 15 45.1	85 48 31	I	1963	12.1	< 0.36	...	< 0.30	...	< 0.30	...	< 0.63	...	...
NGC 2388	07 25 37.9	33 55 21	I	4134	14.7	0.82	0.09	2.64	0.28	17.42	1.90	25.64 <sup>4</sup>	3.80	10.93
NGC 2389	07 25 48.9	33 57 55	I	3957	13.4	0.53	0.07	0.73	0.10	3.40	0.35	5.85 <sup>4</sup>	0.88	10.21
CGCG 058-004	07 32 43.5	11 49 42	I	4984	15.6	< 0.30	...	0.45	0.15	1.56	0.30	2.22	1.21	10.04
UGC 3924	07 32 51.9	11 38 02	O	5163	14.7	< 0.30	...	< 0.30	...	< 0.30	...	< 0.30	...	...
MCG +02-20-002 = NGC 2416	07 32 55.7	11 43 33	I	5101	14.1	< 0.30	...	< 0.50	...	1.39	0.15	2.68	0.50	10.06
MCG +02-20-003	07 32 57.1	11 49 14	I	4873	15.0	< 0.17	...	0.73	0.15	8.81	0.30	12.8	1.40	10.77
ESO 163-G010	07 36 46.7	-55 04 08	O	2798	...	< 0.20	...	< 0.21	...	1.76	0.38	...	...	...
ESO 163-G011	07 36 59.4	-55 04 38	I	2822	11.9	0.37	0.11	0.63	0.15	5.32	1.65	14.64	1.05	10.20
ESO 432-IG006	08 42 25.6	-31 30 48	I	4846	16.4	0.88	0.09	1.14	0.11	7.15	0.73	9.91	1.00	10.67
ESO 564-G010	09 00 29.0	-20 31 00	O	...	14.7	< 0.20	...	< 0.30	...	...	...	...	...	...
ESO 564-G011	09 00 30.0	-20 31 36	I	2596	14.5	0.38	0.05	1.45	0.17	9.17	1.00	11.85	1.20	...
IRAS 0911-1006 e	09 11 10.7	-10 07 03	O	16449	...	< 0.20	...	0.67	0.07	7.39	0.70	13.31	1.40	11.79
IRAS 0911-1006 w	09 11 13.0	-10 06 54	O	16449	...	...	...	...	...	...	...	...	...	...
NGC 2798 = Arp 283	09 14 10.0	42 12 35	I	1739	13.0	0.87	0.09	3.20	0.20	19.29	0.20	27.98	0.96	10.22
NGC 2799	09 14 17.7	42 12 14	O	1755	14.3	< 0.30	...	< 0.40	...	< 1.50	...	< 1.00	...	...
NGC 2854	09 20 38.5	49 25 15	I	2741	13.8	0.20	0.05	0.41	0.10	2.49	0.25	5.29	0.42	9.79
NGC 2856	09 20 54.6	49 27 48	I	2638	14.1	0.43	0.04	1.24	0.07	6.27	0.69	11.57	0.93	10.13
NGC 2857	09 21 13.3	49 34 36	I	4887	12.9	0.15	0.03	0.22	0.08	0.91	0.10	2.78	0.25	9.94
MCG +08-18-012	09 33 12.0	48 41 41	O	...	15.0	< 0.10	...	< 0.24	...	< 1.0	...	...	...	...
MCG +08-18-013	09 33 18.8	48 41 57	I	7777	15.0	< 0.20	...	0.79	0.24	6.23	0.45	9.34	0.67	11.03
NGC 2992 = Arp 245	09 43 17.3	-14 08 39	I	2314	13.1	0.74	0.07	1.57	0.17	7.34	0.80	11.60 <sup>4</sup>	3.00	10.06
NGC 2993	09 43 23.6	-14 08 12	I	2420	13.1	0.58	0.06	1.88	0.20	10.92	1.10	14.64 <sup>4</sup>	3.80	10.25
IC 563 = Arp 303	09 43 44.6	03 16 34	I	6093	14.8	0.38	0.05	< 0.18	...	2.41 <sup>4</sup>	0.20	5.87 <sup>4</sup>	0.60	10.50
IC 564	09 43 45.3	03 18 07	I	6056	14.1	0.30	0.05	0.24	0.04	3.07 <sup>4</sup>	0.25	6.56 <sup>4</sup>	0.70	10.57
IC 2522	09 52 57.1	-32 53 55	I	3012	12.6	0.89	0.23	0.94	0.13	5.15	0.22	13.32	1.24	10.23
IC 2523	09 52 58.9	-32 58 17	I	2611	13.6	< 0.54	0.23	0.32	0.13	2.74	0.22	6.03	1.01	9.80
IC 2545 <sup>5</sup>	10 03 52.2	-33 38 23	I	10230	15.0	0.38	0.11	1.29	0.22	9.71	0.34	9.60	0.46	11.41
NGC 3165	10 10 55.8	03 37 25	O	1332	14.5	< 0.15	...	< 0.30	...	< 0.10	...	< 0.55	...	...
NGC 3166	10 11 09.3	03 40 25	I	1345	11.3	0.51	0.30	0.76	0.06	5.98	0.04	12.57	0.14	9.55
NGC 3169	10 11 38.7	03 43 03	I	1233	11.1	1.31	0.04	1.74	0.04	8.24	0.03	23.59	0.12	9.68
NGC 3226 = UGC 5617	10 20 43.2	20 09 06	O	1151	12.3	< 0.27	...	< 0.18	...	< 0.60	...	...	...	...
NGC 3227 = UGC 5620	10 20 47.3	20 07 03	I	1157	11.1	1.11	0.12	2.04	0.21	9.01	1.00	19.11	2.00	9.60

TABLE 1—*Continued*

Name	RA (B1950) H M S	DEC (B1950) d m "	PT	cz km/s	m <sub>z</sub>	12μm Jy	σ <sub>12</sub> Jy	25μm Jy	σ <sub>25</sub> Jy	60μm Jy	σ <sub>60</sub> Jy	100μm Jy	σ <sub>100</sub> Jy	L <sub>fir</sub> L <sub>⊙</sub>
NGC 3262	10 26 57.5	-43 54 13	O	2864	14.2	< 0.35	...	< 0.42	...	< 0.25	...	< 0.6	...	...
NGC 3263	10 27 04.8	-43 51 54	I	2842	12.5	0.86	0.19	0.93	0.22	8.88	0.36	17.30	1.03	10.36
NGC 3395 = UGC 5931 = Arp 270	10 47 02.6	33 14 44	I	1620	12.4	0.28	0.05	0.72	0.08	6.79 <sup>4</sup>	2.10	13.00 <sup>4</sup>	3.00	9.75
NGC 3396	10 47 08.9	33 15 18	I	1625	12.6	0.23	0.04	0.98	0.11	6.15 <sup>4</sup>	2.10	9.56 <sup>4</sup>	3.00	9.67
NGC 3413	10 48 34.0	33 01 56	I	645	13.1	< 0.10	...	< 0.17	...	1.37	0.40	2.15	0.10	8.22
NGC 3424	10 49 00.1	33 09 54	I	1501	13.2	0.59	0.04	0.94	0.04	9.03	0.09	17.03	0.21	9.81
NGC 3430	10 49 25.2	33 13 03	I	1585	12.2	0.38	0.08	0.78	0.05	4.36	0.07	10.88	1.00	9.59
UGC 6016	10 51 12.1	54 33 13	O	1493	17.0	< 0.10	...	< 0.15	...	< 0.50	...	< 0.50	...	...
NGC 3448	10 51 39.6	54 34 27	I	1350	12.5	0.34	0.11	0.76	0.21	6.74	0.35	12.17	0.47	9.58
ESO 264-G057	10 56 45.8	-43 10 26	I	5156	15.0	0.37	0.10	0.95	0.23	6.78	0.34	17.10	3.20	10.81
ESO 264-G058	10 56 48.2	-43 06 00	I	6120	17.0	< 0.30	...	< 0.30	...	0.61	0.18	< 1.50	...	...
NGC 3511	11 00 57.0	-22 49 00	I	1106	11.5	0.92	0.11	1.16	0.13	9.34	0.13	23.93	0.41	9.62
NGC 3513	11 01 19.2	-22 58 28	I	1194	11.9	< 0.12	...	< 0.48	...	3.27	0.06	7.69	0.23	9.21
MCG +07-23-019 = VV32	11 01 06.8	41 07 12	I	10356	...	< 0.30	...	0.42	0.13	6.57	0.19	11.38	0.44	11.33
IC 2810 = UGC 6436a	11 23 08.4	14 57 08	O	10243	14.9	< 0.25	...	< 0.35	...	5.10 <sup>4</sup>	1.00	10.98	0.30	...
IC 2810b = UGC 6436b	11 23 13.0	14 56 39	O	10240	15.4	< 0.25	...	< 0.41	...	2.10 <sup>4</sup>	1.00	...	...	...
NGC 3690 = Arp 299	11 25 42.0	58 50 17	I	3131	11.8	3.90	0.40	24.14	2.40	121.64	12.50	122.45	12.50	11.48
NGC 3893	11 46 01.8	48 59 13	I	973	11.2	1.7	0.19	2.09	0.33	15.76	0.17	38.38	0.53	9.72
NGC 3896	11 46 26.8	49 01 39	O	869	13.9	< 0.21	...	< 0.18	...	< 0.33	...	< 0.30	...	...
NGC 3991 = Arp 313	11 54 54.0	32 36 00	I	3111	14.2	< 0.12	...	0.21	0.04	2.92	0.28	4.22	0.45	9.90
NGC 3994	11 55 02.3	32 33 23	I	3096	13.3	0.32	0.04	0.46	0.05	4.98	0.50	10.31	1.20	10.19
NGC 3995	11 55 10.3	32 34 24	I	3254	12.7	< 0.18	...	0.64	0.07	3.75	0.30	6.63	0.68	10.08
NGC 4038 <sup>2</sup>	11 59 20.0	-18 35 49	I	1642	10.9	2.92	0.38	7.11	1.13	46.88	1.70	85.69	8.20	10.59
ESO 440-IG058 = VV 835	12 04 17.3	-31 40 17	I	6818	16.0	0.37	0.06	0.97	0.09	7.30	0.78	13.40	1.50	11.02
NGC 4169	12 09 47.0	29 27 30	O	3784	13.2	< 0.35	...	< 0.30	...	< 0.33	...	< 0.80	...	...
NGC 4170	12 09 50.2	29 28 57	O	1127	13.6	< 0.30	...	< 0.10	...	< 0.30	...	< 0.80	...	...
NGC 4174	12 09 54.9	29 25 36	O	3980	14.3	< 0.24	...	< 0.33	...	< 0.21	...	< 1.20	...	...
NGC 4175	12 09 58.6	29 26 52	I	3956	14.2	0.40	0.13	0.77	0.26	5.70	0.31	10.58	0.61	10.44
ESO 267-G029	12 11 15.0	-46 59 47	I	5445	14.2	0.23	0.09	0.82	0.15	5.17	0.20	9.05	0.96	10.67
ESO 267-G030	12 11 34.8	-46 56 56	I	5543	14.2	0.32	0.09	0.75	0.13	4.73	0.18	10.91	0.91	10.70
IC 3153	12 17 03.8	05 40 33	I	11646	14.8	< 0.20	...	< 0.20	...	0.60	0.18	1.32	0.41	10.38
NGC 4266	12 17 08.2	05 49 06	I	2495	14.6	< 0.20	...	< 0.30	...	0.31	0.1	2.09	1.31	9.10
NGC 4268	12 17 13.9	05 33 40	O	2374	13.8	< 0.20	...	< 0.20	...	< 0.30	...	< 0.51	...	...
NGC 4270	12 17 16.2	05 44 27	O	2357	13.1	< 0.20	...	< 0.30	...	< 0.50	...	< 0.33	...	...
NGC 4273	12 17 23.6	05 37 13	I	2378	12.4	1.05	0.34	1.35	0.39	11.27	0.25	21.87	1.31	10.31
NGC 4277	12 17 30.5	05 37 07	O	2516	13.4	< 0.20	...	< 0.20	...	< 0.60	...	< 1.20	...	...
NGC 4281	12 17 48.6	05 39 54	I	2711	12.3	< 0.20	...	< 0.40	...	0.83	0.15	1.78	0.51	9.31
NGC 4485 = Arp 269	12 28 03.3	41 58 26	I	493	12.3	< 0.90	...	0.53	0.10	2.16	0.70	3.83	1.05	8.21
NGC 4490	12 28 08.9	41 55 26	I	578	10.2	2.74	0.14	5.34	0.80	50.86	6.00	88.29	1.05	9.71
NGC 4567/8 <sup>2</sup>	12 34 02.3	11 31 06	I	2260	11.1	2.1	0.25	2.93	0.74	21.11	0.25	56.77	1.25	10.60
IC 3639	12 38 10.2	-36 28 45	I	3285	13.0	0.82	0.10	2.87	0.30	8.27	1.00	14.90	1.20	...
ESO 381-G009	12 38 16.5	-36 27 05	I	3050	13.9	< 0.16	...	0.32	0.10	1.17	0.15	...	...	...
NGC 4627	12 39 33.5	32 50 51	O	765	13.1	< 0.27	...	< 0.24	...	< 0.50	...	< 1.80	...	...
NGC 4631	12 39 40.7	32 48 54	I	606	09.8	6.81	0.25	11.24	0.68	99.69	3.50	193.26	4.10	10.07
NGC 4647	12 41 01.0	11 51 20	I	1414	11.9	0.76	0.08	1.06	0.16	6.04	0.24	17.56	0.81	9.67
NGC 4649	12 41 08.4	11 49 35	O	1114	9.8	0.33	0.05	< 0.32	...	< 0.24	...	< 1.05	...	...
NGC 4922 a/b	12 59 01.7	29 35 00	I	7071	14.2	0.22	0.08	1.67	0.27	6.01	1.22	7.78	0.67	10.91

TABLE 1—*Continued*

Name	RA (B1950) H M S	DEC (B1950) d m ''	PT	cz km/s	m <sub>z</sub>	12μm Jy	σ <sub>12</sub> Jy	25μm Jy	σ <sub>25</sub> Jy	60μm Jy	σ <sub>60</sub> Jy	100μm Jy	σ <sub>100</sub> Jy	L <sub>far</sub> L <sub>⊙</sub>
MCG -02-33-098	12 59 41.6	-15 29 54	I	4773	14.5	< 0.33	...	1.95	0.39	7.82	0.23	10.29	0.85	10.69
MCG -02-33-099	12 59 49.1	-15 30 36	O	5019	18.0	< 0.10	...	< 0.30	...	< 0.20	...	< 0.50	...	...
UGC 8335 Ned01 = VV250b = Arp238	13 13 36.3	62 23 32	O	9453	15.0	< 0.30	...	< 0.50	...	...	...	...	...	...
UGC 8335 Ned02 = VV250a	13 13 41.4	62 23 21	I	9313	15.0	0.49	0.05	2.08	0.20	11.45	1.30	12.90	1.30	11.41
IC 879	13 16 55.2	-27 10 12	I	1969	14.0	0.23	0.05	0.52	0.08	0.74	0.08	< 0.29	...	...
NGC 5078	13 17 04.6	-27 08 51	I	2168	11.8	1.20	0.13	1.36	0.15	10.37	1.10	35.84	5.70	10.32
MCG -03-34-063	13 19 38.3	-16 26 50	O	6394	15.0	< 0.45	...	< 0.4	...	3.03 <sup>4</sup>	1.05	3.90 <sup>4</sup>	1.10	10.34
MCG -03-34-064	13 19 43.6	-16 28 05	O	4959	14.6	0.84	0.24	3.08	0.36	4.63 <sup>4</sup>	1.13	2.80 <sup>4</sup>	1.10	10.44
NGC 5216 = UGC 8528	13 30 23.0	63 01 32	I	2949	13.6	< 0.09	...	< 0.18	...	0.19	0.03	< 0.05	...	...
NGC 5218 = UGC 8529	13 30 27.1	63 01 32	I	2860	13.1	0.36	0.03	0.92	0.08	7.14	0.70	14.38	1.44	10.28
NGC 5257 = Arp 240	13 37 19.7	01 05 33	O	6798	12.9	0.52 <sup>4</sup>	0.16	1.18 <sup>4</sup>	0.30	8.10 <sup>4</sup>	2.00	13.63 <sup>4</sup>	3.00	11.05
NGC 5258	13 37 24.6	01 05 06	O	6757	12.9	0.25 <sup>4</sup>	0.10	0.78 <sup>4</sup>	0.30	3.94 <sup>4</sup>	1.00	7.27 <sup>4</sup>	1.80	10.75
NGC 5331 <sup>2</sup>	13 49 43.4	02 20 60	I	9906	13.7	< 0.30	...	0.79	0.15	6.27	0.33	10.71	0.50	11.27
NGC 5394 = UGC 8898 = Arp 84	13 56 22.5	37 42 00	I	3427	13.7	0.52	0.05	1.19	0.11	5.62 <sup>4</sup>	1.41	10.43 <sup>4</sup>	3.10	10.31
NGC 5395	13 56 29.3	37 40 03	I	3487	12.1	0.40	0.04	0.48	0.06	6.86 <sup>4</sup>	1.50	14.21 <sup>4</sup>	3.10	10.44
IC 4356	13 56 36.6	37 43 59	O	...	16.2	< 0.20	...	< 0.27	...	< 0.45	...	< 0.10	...	...
NGC 5426 = Arp 271	14 00 47.7	-05 49 47	I	2621	12.7	< 0.70	...	< 0.90	...	3.30	0.37	8.58	1.52	9.92
NGC 5427	14 00 48.6	-05 47 27	I	2618	11.9	0.74	0.09	0.96	0.10	7.50	0.80	16.47	3.32	10.24
NGC 5506	14 10 39.1	-02 58 26	I	1815	13.4	1.48	0.09	4.29	0.15	8.82	0.10	8.96	0.12	9.87
NGC 5507	14 10 43.9	-02 54 55	O	1852	13.6	< 0.16	...	< 0.28	...	< 0.38	...	< 0.66	...	...
NGC 5595	14 21 28.4	-16 29 55	I	2691	13.1	0.67	0.04	0.98	0.05	8.84	0.04	17.23	0.14	10.31
NGC 5597	14 21 42.2	-16 32 19	I	2619	12.6	0.63	0.04	1.85	0.06	8.90	0.06	15.30	0.16	10.27
NGC 5734	14 42 19.0	-20 39 36	I	4074	13.7	0.78	0.15	0.98	0.07	8.09	0.15	17.48	2.45	10.65
NGC 5743	14 42 20.0	-20 42 12	I	4216	13.8	0.59	0.13	0.75	0.08	5.21	0.15	9.78	1.27	10.46
IC 4518 A/B	14 54 26.0	-42 55 54	I	4921	15.0	0.53	0.05	1.52	0.15	9.59	1.00	22.22	2.30	10.90
UGC 9618 Ned 2 = VV 340	14 54 47.8	24 49 05	I	10173	14.6	0.53 <sup>2</sup>	0.13	0.66	0.18	7.08	2.00	15.48	5.00	11.39
UGC 9618 Ned 1	14 54 48.1	24 48 21	O	9776	15.3	...	...	< 0.21	...	< 1.50	...	< 5.00	...	...
NGC 5793	14 56 37.1	-16 29 40	I	3491	14.2	0.25	0.04	0.68	0.07	6.14	0.22	10.57	0.19	10.35
NGC 5796	14 56 36.5	-16 25 30	O	2962	12.7	< 0.25	...	< 0.30	...	< 0.36	...	< 0.35	...	...
IZw107	15 16 19.7	42 55 36	I	12043	15.0	0.31	0.09	1.47	0.14	9.57	0.19	10.75	0.35	11.56
NGC 5915	15 18 47.7	-12 54 56	I	2291	13.0	0.74	0.04	1.84	0.05	11.71	0.05	17.45	0.22	10.25
NGC 5916a	15 18 28.9	-12 55 29	I	2338	14.6	< 0.60	...	< 0.90	...	0.79	0.04	< 1.50	...	...
NGC 5916	15 18 52.0	-12 59 37	I	2338	14.2	< 0.15	...	< 0.24	...	1.11	0.06	3.04	0.35	9.42
NGC 5929	15 24 18.9	41 50 41	O	2561	14.1	< 0.24	...	< 0.30	...	< 1.00	...	...	...	...
NGC 5930	15 24 20.7	41 51 00	O	2672	13.6	0.45	0.09	1.84	0.19	9.71	0.19	14.71	0.66	10.30
NGC 5953	15 32 13.7	15 21 43	I	1965	13.3	0.72	0.12	1.85	0.11	12.00	0.16	21.18	0.85	10.15
NGC 5954	15 32 15.7	15 22 10	O	1959	13.7	< 0.15	...	< 0.40	...	...	...	...	...	...
NGC 6285	16 57 36.1	59 01 53	I	5691	15.3	0.20	0.05	0.27	0.05	2.60 <sup>4</sup>	0.60	6.60 <sup>4</sup>	2.30	10.48
NGC 6286	16 57 45.0	59 00 41	I	5501	14.1	0.45	0.06	0.55	0.06	8.03 <sup>4</sup>	2.00	18.30 <sup>4</sup>	4.00	10.92
IC 4686/7 <sup>5</sup>	18 09 19.4	-57 44 28	I	5200	13.8	0.94	0.20	2.96	0.20	16.08 <sup>4</sup>	1.35	28.55	1.09	11.12
IC 4689	18 09 22.1	-57 45 45	I	4949	15.0	< 0.25	...	0.71	0.20	5.00 <sup>4</sup>	1.20	...	...	...
NGC 6621 = Arp 81	18 13 09.3	68 20 50	I	6284	14.0	0.31	0.05	1.02	0.10	7.02	1.20	12.19	2.30	10.93
NGC 6622	18 13 14.4	68 20 15	O	6230	16.0	< 0.12	...	< 0.30	...	< 1.00	...	< 1.30	...	...
CGCG 142 - 033 = Zwicky 142	18 14 24.0	22 05 00	O	5353	15.6	< 0.20	...	< 0.30	...	< 0.30	...	< 1.00	...	...
CGCG 142 - 034	18 14 32.6	22 05 36	I	5599	15.6	0.27	0.06	0.64	0.08	6.55	0.80	13.25	1.60	10.82

TABLE 1—*Continued*

Name	RA (B1950) H M S	DEC (B1950) d m "	PT	cz km/s	m <sub>s</sub>	12μm Jy	σ <sub>12</sub> Jy	25μm Jy	σ <sub>25</sub> Jy	60μm Jy	σ <sub>60</sub> Jy	100μm Jy	σ <sub>100</sub> Jy	L <sub>fir</sub> L <sub>⊙</sub>
NGC 6670	18 32 56.4	59 50 58	I	8650	...	0.47	0.05	1.10	0.10	9.24	0.90	14.84	1.50	11.31
CGCG 301-032	18 33 32.8	59 49 14	I	8699	15.2	0.15	0.04	0.15	0.04	0.90	0.10	1.64	0.18	10.32
NGC 6745	19 00 03.3	40 40 23	I	4545	13.3	0.45	0.05	0.92	0.12	6.84	0.70	13.01	1.40	10.65
NGC 6786 = VV 414	19 11 52.9	73 19 31	I	7510	13.8	0.15	0.04	0.55	0.05	3.40 <sup>4</sup>	0.60	6.11 <sup>4</sup>	1.40	10.77
UGC 11415	19 12 04.0	73 20 27	I	7555	14.9	0.21	0.04	0.91	0.09	4.51 <sup>4</sup>	0.84	5.89 <sup>4</sup>	1.40	10.85
NGC 6921	20 26 20.8	25 33 23	O	4391	14.4	< 0.25	...	0.62	0.20	3.97	1.20	7.48	2.30	10.38
MCG +04-48-002	20 26 26.8	25 34 00	O	4259	18.0	0.51	0.09	0.71	0.20	8.15	1.20	12.50	2.70	10.63
NGC 6926	20 30 29.8	-02 12 01	I	5970	13.2	0.66	0.11	0.91	0.18	7.85	0.33	18.50	1.64	10.99
NGC 6929	20 30 45.9	-02 12 31	O	6174	14.4	< 0.50	...	< 0.40	...	< 0.50	...	< 0.50	...	...
ESO 286-IG033	21 00 50.6	-43 43 59	I	4990	...	...	...	0.43	0.08	1.33	0.10	1.42	0.17	9.93
ESO 286-IG035	21 00 52.7	-43 47 31	I	5208	14.7	...	...	1.12	0.14	8.17	0.90	14.16	1.60	10.83
NGC 7172	21 59 07.1	-32 06 42	I	2575	12.9	0.72	0.06	1.06	0.11	6.06	0.61	15.10	1.35	10.16
NGC 7174/6	21 59 11.9	-32 14 03	I	2778	12.2	0.25	0.04	0.61	0.06	3.65	0.40	10.15	1.00	10.03
NGC 7253 = Arp 278 <sup>2</sup>	22 17 11.7	29 08 41	I	4718	14.4	0.43	0.05	0.70	0.09	6.38	0.70	13.63	1.50	10.67
NGC 7469	23 00 44.4	08 36 19	I	4916	13.0	1.63	0.35	5.70	0.19	23.13	0.64	39.91	1.36	11.22
IC 5283	23 00 47.0	08 37 26	O	4894	14.8	< 0.30	...	< 0.31	...	...	...	...	...	...
NGC 7537	23 12 00.9	04 13 21	I	2674	13.9	< 0.45	...	< 0.60	...	1.25	0.18	1.67	0.64	9.39
NGC 7541	23 12 11.8	04 15 36	I	2678	12.4	1.34	0.24	2.36	0.32	20.81	0.75	43.95	1.59	10.69
NGC 7552	23 13 25.4	-42 51 27	I	1585	11.3	3.49	0.36	12.43	1.40	78.38	8.00	104.85	12.00	10.73
NGC 7582	23 15 38.3	-42 31 54	I	1575	11.4	2.54	0.30	9.43	1.10	52.25	5.60	87.60	9.30	10.59
NGC 7590	23 16 10.3	-42 30 45	I	1596	12.1	1.02	0.10	1.23	0.14	8.54	0.90	19.57	2.40	9.87
NGC 7599	23 16 35.9	-42 31 54	I	1654	12.1	1.06	0.10	1.40	0.18	6.95	1.40	19.45	2.00	9.86
NGC 7592	23 15 47.4	-04 41 26	I	7328	11.4	0.62	0.19	1.26	0.30	7.81	0.36	10.66	0.99	11.07
ESO 077-IG 014	23 17 58.5	-69 29 28	I	11400	16.5	< 0.23	...	0.61	0.17	6.02	0.35	10.62	1.41	11.38
NGC 7714 = UGC 12699	23 33 41.0	01 52 34	I	2798	13.0	0.56	0.05	3.15	0.30	10.73	1.10	12.46	1.30	10.34
NGC 7715	23 33 48.5	01 52 48	O	2770	14.7	< 0.15	...	< 0.21	...	< 0.15	...	< 0.40	...	...
MCG -01-60-021	23 39 11.6	-03 56 46	I	6595	16.5	< 0.27	...	< 0.20	...	0.81	0.31	1.42	0.31	10.03
MCG -01-60-022	23 39 27.1	-03 53 33	I	6966	14.5	0.37	0.13	0.78	0.08	5.11	0.32	9.45	0.31	10.89
NGC 7752	23 44 27.1	29 10 52	O	5072	15.0	0.64	0.05	0.54	0.15	3.96	1.31	8.02	2.41	10.52
NGC 7753	23 44 33.3	29 12 21	O	5163	12.8	...	...	0.34	0.15	2.68	0.88	8.87	2.30	10.47
NGC 7769	23 48 32.2	19 52 23	I	4214	12.8	0.52	0.04	0.97	0.08	5.21	0.40	13.58	1.40	10.53
NGC 7771	23 48 51.7	19 49 52	I	4287	13.1	1.23	0.16	2.90	0.22	20.93	1.78	44.85	3.80	11.11
UGC 12812	23 48 45.8	20 18 00	O	5326	15.5	< 0.25	...	< 0.30	...	< 1.00	...	< 1.30	...	...
Mrk 331 = MCG +03-60-036	23 48 53.6	20 18 24	I	5541	14.9	0.87	0.13	3.02	0.24	18.43	1.60	22.56	2.50	11.18
UGC 12914	23 59 04.0	23 12 23	O	4371	13.1	< 0.14	...	< 0.60	...	2.52	0.70	4.05	1.90	10.15
UGC 12915	23 59 08.6	23 12 59	O	4336	14.0	0.36	0.06	1.16	0.24	5.18	1.70	13.05	2.80	10.54

NOTE.—Upper limits for galaxies which would have been separated had they been detected are indicated with a < symbol, with the associated 1-σ value having no data. For cases when galaxies were unresolved, the integrated HIRES flux (sum of all galaxy components) is given for the component dominant at other IRAS wavelengths, with the remaining components having no data for either their fluxes or their uncertainties. Specific Notes - (1) bad scan (2) flux lies between galaxies (3) dense cluster (4) resolved using component fitting (5) except NGC 7319/7320



TABLE 2  
INTEGRATED FLUX DENSITIES OF RBGS INTERACTING GALAXIES

Name	RA (B1950) H M S	DEC (B1950) d m s	PT	cz km/s	m <sub>z</sub>	12μm Jy	σ <sub>12</sub> Jy	25μm Jy	σ <sub>25</sub> Jy	60μm Jy	σ <sub>60</sub> Jy	100μm Jy	σ <sub>100</sub> Jy	L <sub>fir</sub> L <sub>⊙</sub>
NGC 274	00 48 30.0	-07 19 45	O	1750	12.8	< 0.40	...	< 0.25	...	< 1.20	...	...	...	...
NGC 275	00 48 33.0	-07 20 09	I	1750	13.2	< 0.40	...	0.91	0.08	5.38	0.40	9.54	1.15	9.70
NGC 1143 = UGC 2388 = Arp 118	02 52 36.2	-00 22 47	O	8459	13.2	< 0.30	...	< 0.10	...	< 1.10	...	< 1.50	...	...
NGC 1144 = UGC 2389	02 52 38.6	-00 23 11	I	8647	13.8	0.44	0.05	0.85	0.08	5.70	0.68	11.75	1.72	11.14
UGC 3094	04 32 39.0	19 04 12	I	7408	16.5	0.60	0.06	1.10	0.10	7.16	0.72	16.39	1.70	11.13
2MASX J04354305+1909568	04 32 47.8	19 03 51	O	...	...	< 0.12	...	< 0.22	...	< 0.28	...	< 2.00	...	...
IRAS 15335-0513	15 33 32.6	-05 13 55	I	8186	16.7	< 0.23	...	0.88	0.10	5.83	0.60	10.10	1.00	11.07
2MASX J15360897-0521513	15 36 08.9	-05 21 52	O	7077	16.6	< 0.12	...	< 0.15	...	< 0.25	...	< 0.30	...	...
NGC 6907/8	20 22 08.0	-24 58 17	I	3161	11.9	1.29	0.13	2.42	0.25	14.76	1.50	31.78	3.50	10.69

NOTE.—When a target was unresolved, the integrated HIRES flux (sum of all galaxy components) is given for the component dominant at other wavelengths, with the remaining components having no data. Upper limits are indicated with a < symbol, with the associated 1-σ values blank. See text for detailed explanation of columns.